



Article

Molecular Hybridization Strategy on the Design, Synthesis, and Structural Characterization of Ferrocene-*N*-acyl Hydrazones as Immunomodulatory Agents

Laís Peres Silva ¹, Ivanilson Pimenta Santos ², Dahara Keyse Carvalho Silva ², Bruna Padilha Zurita Claro dos Reis ², Cássio Santana Meira ^{1,2,3}, Marcos Venícius Batista de Souza Castro ⁴, José Maurício dos Santos Filho ⁴, João Honorato de Araujo-Neto ⁵ , Javier Alcides Ellena ⁵, Rafael Gomes da Silveira ^{5,6}  and Milena Botelho Pereira Soares ^{2,3,*}

¹ Department of Life Sciences, State University of Bahia (UNEB), Salvador 41150-000, BA, Brazil

² Gonçalo Moniz Institute, Oswaldo Cruz Foundation (IGM-FIOCRUZ/BA), Salvador 40296-710, BA, Brazil

³ Institute for Innovation in Advanced Health Systems (CIMATEC ISI SAS—University Center SENAI/CIMATEC), Salvador 41650-010, BA, Brazil

⁴ Laboratory of Design and Synthesis Applied to Medicinal Chemistry-SintMed®, Center for Technology and Geosciences, Federal University of Pernambuco, Recife 50740-521, PE, Brazil

⁵ Multiuser Laboratory of Structural Crystallography, Institute of São Carlos, University of São Paulo, São Carlos 13566-590, SP, Brazil

⁶ Department of Chemistry, Federal Institute of Goiás, Campus Ceres, Ceres 76300-000, GO, Brazil

* Correspondence: milena.soares@fiocruz.br



Citation: Silva, L.P.; Santos, I.P.; Silva, D.K.C.; dos Reis, B.P.Z.C.; Meira, C.S.; Castro, M.V.B.d.S.; dos Santos Filho, J.M.; Araujo-Neto, J.H.d.; Ellena, J.A.; Silveira, R.G.d.; et al. Molecular Hybridization Strategy on the Design, Synthesis, and Structural Characterization of Ferrocene-*N*-acyl Hydrazones as Immunomodulatory Agents. *Molecules* **2022**, *27*, 8343. <https://doi.org/10.3390/molecules27238343>

Academic Editor: Giuseppe Manfroni

Received: 26 September 2022

Accepted: 22 November 2022

Published: 30 November 2022

Publisher's Note: MDPI stays neutral with regard to jurisdictional claims in published maps and institutional affiliations.



Copyright: © 2022 by the authors. Licensee MDPI, Basel, Switzerland. This article is an open access article distributed under the terms and conditions of the Creative Commons Attribution (CC BY) license (<https://creativecommons.org/licenses/by/4.0/>).

Abstract: Immunomodulatory agents are widely used for the treatment of immune-mediated diseases, but the range of side effects of the available drugs makes necessary the search for new immunomodulatory drugs. Here, we investigated the immunomodulatory activity of new ferrocenyl-*N*-acyl hydrazones derivatives (**SintMed(141–156)**). The evaluated *N*-acyl hydrazones did not show cytotoxicity at the tested concentrations, presenting CC_{50} values greater than 50 μ M. In addition, all ferrocenyl-*N*-acyl hydrazones modulated nitrite production in immortalized macrophages, showing inhibition values between 14.4% and 74.2%. By presenting a better activity profile, the ferrocenyl-*N*-acyl hydrazones **SintMed149** and **SintMed150** also had their cytotoxicity and anti-inflammatory effect evaluated in cultures of peritoneal macrophages. The molecules were not cytotoxic at any of the concentrations tested in peritoneal macrophages and were able to significantly reduce ($p < 0.05$) the production of nitrite, TNF- α , and IL-1 β . Interestingly, both molecules significantly reduced the production of IL-2 and IFN- γ in cultured splenocytes activated with concanavalin A. Moreover, **SintMed150** did not show signs of acute toxicity in animals treated with 50 or 100 mg/kg. Finally, we observed that ferrocenyl-*N*-acyl hydrazone **SintMed150** at 100 mg/kg reduced the migration of neutrophils (44.6%) in an acute peritonitis model and increased animal survival by 20% in an LPS-induced endotoxic shock model. These findings suggest that such compounds have therapeutic potential to be used to treat diseases of inflammatory origin.

Keywords: immunomodulation; endotoxic shock; acute peritonitis; *N*-acyl hydrazones; ferrocene

1. Introduction

Throughout life, the human organism is exposed to a series of agents that can break homeostasis, whether they are pathogenic or not [1]. Among the pathogens, bacteria, fungi, parasites, and viruses stand out, while among the non-pathogenic agents there are trauma, exposure to toxic compounds, radioactivity, and smoke. Exposure to these agents culminates in the emergence of inflammation as the body responds to such harmful stimuli [2]. Inflammation is one of the body's protective and fundamental reactions. It occurs in order to eliminate the source of the noxious stimulus or tissue injury to which the

organism is being subjected and involves a series of cellular and molecular processes that aim to reestablish body homeostasis [3].

Despite its remarkable protective function, the inflammatory process, in addition to being well orchestrated, needs to be well controlled and properly terminated to prevent it from contributing to the emergence of metabolic disorders that may lead to diabetes and cancer, for example [4]. It is reported that unresolved inflammation can lead to the emergence of a series of inflammatory diseases that affect a large part of the population, such as asthma, rheumatoid arthritis, and atherosclerosis [5].

Currently, inflammation is controlled with two classes of drugs widely used in clinical practice: non-steroidal anti-inflammatory agents (NSAIDs) and glucocorticoids [6,7]. Despite their known effectiveness in the treatment of inflammatory disorders, the indiscriminate use of these drugs by the population has been increasing and, along with it, the incidence of adverse effects also grows [6–9]. The frequent use of non-steroidal anti-inflammatory drugs causes a series of unwanted reactions in the body such as gastrointestinal complications, cardiovascular diseases, and kidney diseases, while glucocorticoids can cause cardiovascular disease and disorders such as Cushing's syndrome [8,9].

In this scenario, it is necessary to develop effective drugs with fewer adverse effects for the management of inflammation, and *N*-acyl hydrazones (NAHs) appear as promising alternatives. As a privileged structure in medicinal chemistry [10], the NAH scaffold is often found as a structural part of strong candidates for the control of inflammatory diseases due to their already reported action on macrophages and lymphocyte cells and in experimental models of immune diseases [11–13]. It is a Schiff base resulting from the condensation of carbonylated substances with hydrazides and constitutes a key pharmacophore for the binding and consequent inhibition of cyclooxygenases, acting as NSAIDs [14,15]. In addition, the NAH fraction provides greater stability and a safer inhibition of COX, and it is believed that this occurs from the relative hydrogen acidity of the amine group or its ability to stabilize free radicals [16,17]. As an important concept for the design of potentially bioactive compounds, molecular hybridization is a useful strategy based on the combination of pharmacophoric moieties of diverse substances to lead to a new molecule with an improved biological response when compared to the starting structural models [18,19].

Targeting the development of molecular hybrids that incorporate a second fragment of importance for the desired biological activity and remain structurally simple, the ferrocene (Fc) core was selected for the present studies, since Fc-bearing compounds are recognized for their importance in medicinal chemistry [20]. Ferrocene derivatives have been found to play an important role in the discovery of new immunomodulatory molecules [21–24], especially due to the Fc mechanisms of action, which are usually multi-modal, and rarely accessible with most organic pharmacophores. Some of the well-known mechanisms of action of ferrocene comprise direct protein inhibition, photoactivation with consequent singlet oxygen generation and cellular damage, metalation of macromolecules, and, the most common, redox activation and reactive oxygen species (ROS) formation, leading to cellular oxidative stress [25–27]. Due to the iron presence in the structure and its role in the oxidative biochemical processes, oxidative stress is the most important mechanism of action observed in bioactive ferrocene derivatives, so its association with other pharmacophoric groups has been proven to be an excellent strategy for the design of new potential biological active molecules [28]. Therefore, a series of ferrocene-*N*-acyl hydrazone (Fc-NAH) hybrids has been designed according to the concept in Figure 1, which fulfills our main goal of obtaining simple molecules with an accessible and easy synthetic route as well as the potential for further molecular modifications and biological studies.

Based on this premise, our group carried out the synthesis of new Fc-NAH derivatives and, in the present study, we have investigated their structural characterization by means of spectroscopic and crystallographic techniques, as well as their *in vitro* immunomodulatory activity, and also tested the effectiveness of the most active molecule **SintMed150** in murine models of endotoxic shock and acute peritonitis.

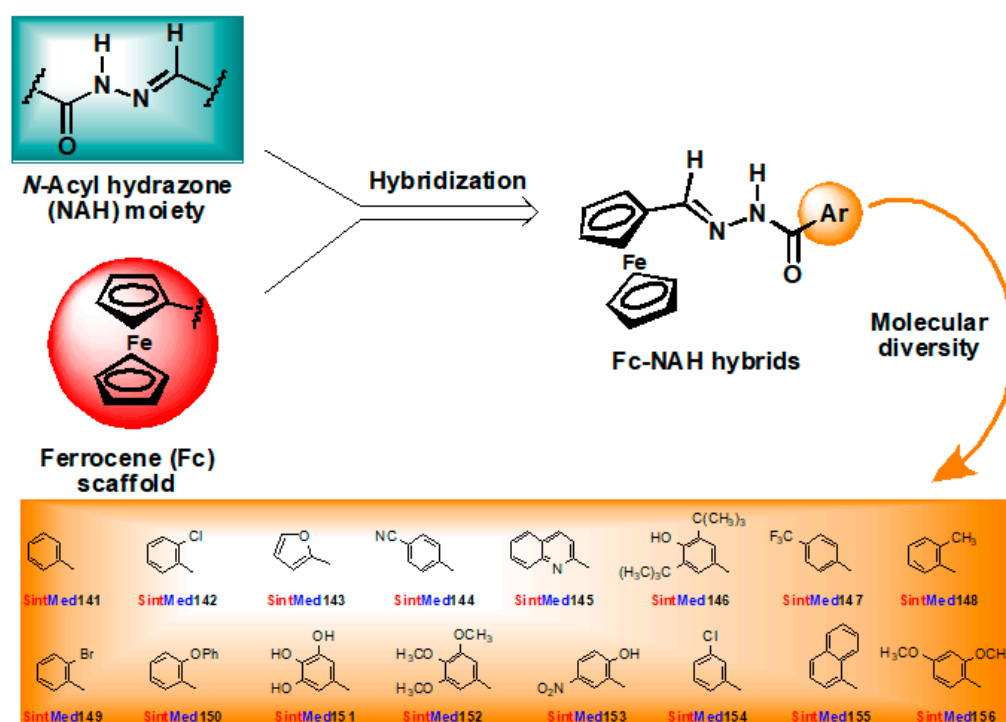


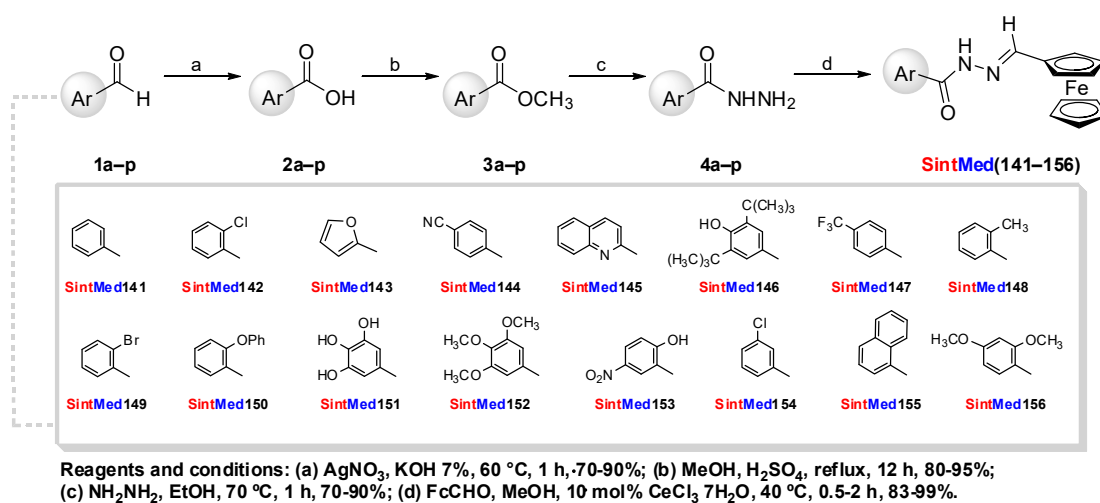
Figure 1. Molecular hybridization strategy applied to the design of ferrocene-*N*-acyl hydrazones (Fc-NAH).

2. Results

The synthetic route to prepare the planned compounds **SintMed(141–156)**, depicted in Scheme 1, was based on a method developed by our research group [29]. Commercially available aldehydes **1a–p** have undergone silver (I)-mediated oxidation under basic conditions [30], leading to the corresponding carboxylic acids **2a–p** as solid materials with good yields. Aryl carboxylic methyl esters **3a–p** were easily obtained by means of Fischer esterification, and thus converted into the corresponding hydrazides **4a–p** under reflux in the presence of hydrazine hydrate in excess. The key intermediate hydrazides **4a–p** and ferrocenecarboxaldehyde were reacted in the presence of cerium (III) chloride heptahydrate ($\text{CeCl}_3 \cdot 7\text{H}_2\text{O}$) as a catalyst under mild conditions, according to a method developed in our laboratory [31], in order to afford the Fc-NAH series **SintMed(141–156)** with excellent isolated yields, stereoselectivity, and high purity of crude products. The Fc-NAH were characterized using spectroscopic techniques such as nuclear magnetic resonance of hydrogen (^1H NMR) and carbon-13 (^{13}C NMR) and infrared spectroscopy (IR), as well as elemental analysis.

In addition to the assessed physical and spectroscopic data, attempts to reinforce the formation of the thermodynamically more stable *E*-isomers by means of the CeCl_3 -catalyzed synthesis of the Fc-NAH have included the crystallographic structure acquisition of some molecules of this series, with success for compound **SintMed149**, one of the more active molecules, confirming the proposed molecular structures and their purity. The *E*-isomer structure is clearly confirmed as observed in Figure 2.

Initially, the cytotoxicity of the molecules was tested in the J774 macrophage cell line. All evaluated ferrocenyl-*N*-acyl hydrazones did not show cytotoxicity at the tested concentrations, exhibiting CC_{50} values greater than 50 μM (Table 1). Under the same conditions, gentian violet, used as a positive control, presented a CC_{50} value equal to 0.8 μM .



Scheme 1. Synthetic route for the ferrocene-*N*-acyl hydrazone derivatives.

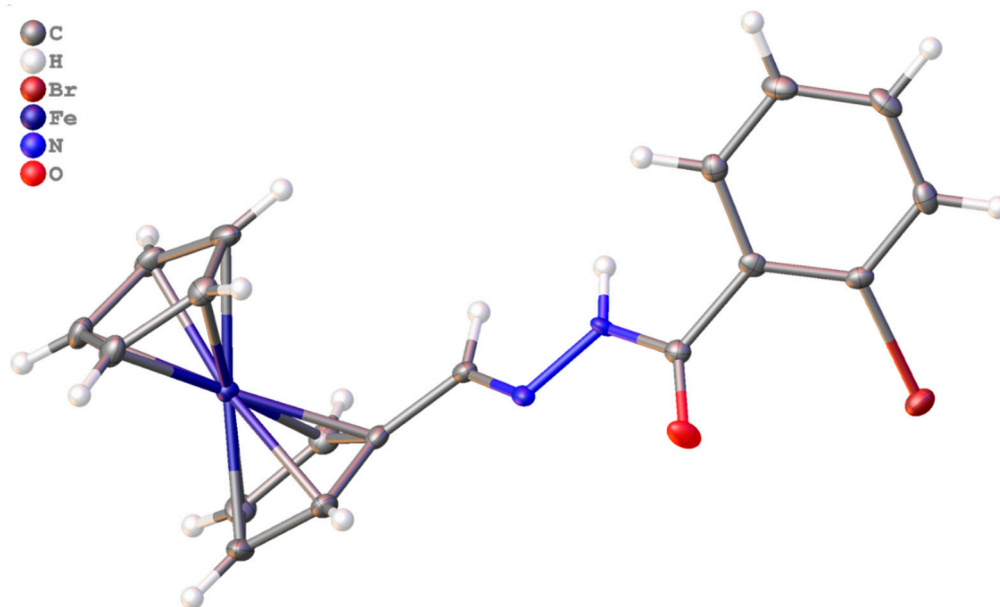
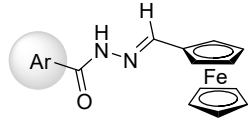


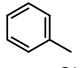
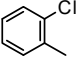
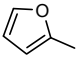
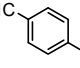
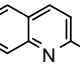
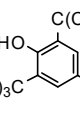
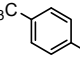
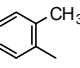
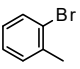
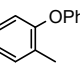
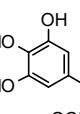
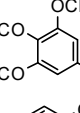
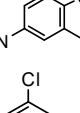
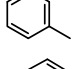
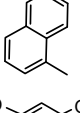
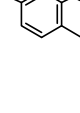
Figure 2. Crystal structure of the complex **SintMed149**. The ellipsoids are represented at 30% of probability.

The anti-inflammatory effect of the molecules was initially evaluated at a concentration of 40 μM in cultures of macrophages stimulated with LPS + IFN- γ by analysis of nitric oxide production. As can be seen in Table 1, all Fc-NAH derivatives modulate nitrite production, showing inhibition values between 14.4% and 74.2%. The most active molecules were the ferrocenyl-*N*-acyl hydrazones **SintMed149** and **SintMed150**, which showed inhibition values of 71.7% and 74.2% respectively. Under the same conditions, dexamethasone (Dexa) showed inhibition of 64.9% (Table 1).

To further explore the anti-inflammatory potential of compounds **SintMed149** and **SintMed150**, a new set of experiments was performed using peritoneal macrophages. Initially, the cytotoxicity of the investigated compounds was evaluated in peritoneal macrophages in the presence of LPS + IFN γ . As revealed in Figure 3, the molecules were not cytotoxic at any of the concentrations tested, as well as dexamethasone at 40 μM .

Table 1. Cytotoxicity and inhibitory effect on nitric oxide production of Fc-NAH SintMed(141–156).



Compounds	R	CC ₅₀ (μM) JJ74 ^a	Inhibition of NO (%) Production at 40 μM ^b
SintMed141		>50	19.7 (±3.0)
SintMed142		>50	49.3 (±0.8)
SintMed143		>50	49.2 (±1.9)
SintMed144		>50	55.2 (±0.6)
SintMed145		>50	49.6 (±2.6)
SintMed146		>50	14.4 (±2.2)
SintMed147		>50	59.9 (±0.3)
SintMed148		>50	56.6 (±2.1)
SintMed149		>50	71.7 (±3.6)
SintMed150		>50	74.2 (±0.7)
SintMed151		>50	25.2 (±2.1)
SintMed152		>50	55.5 (±1.7)
SintMed153		>50	43.7 (±3.3)
SintMed154		>50	45.2 (±2.1)
SintMed155		>50	35.6 (±0.7)
SintMed156		>50	46.7 (±3.0)
GV ^c		0.8 (±0.1)	-
Dexamethasone ^d		-	64.9 (±6.7)

^a Cytotoxicity was evaluated on J774 macrophages exposed to compounds for 72 h by Alamar blue method. ^b Percent inhibition determined 24 h after incubation with compounds and LPS plus IFN- γ . ^c reference cytotoxic drug. ^d reference immunosuppressive drug. Values represent the mean (\pm standard deviation) of three independent experiments. CC₅₀ = cytotoxic concentration at 50%. NO = nitric oxide. GV = gentian violet.

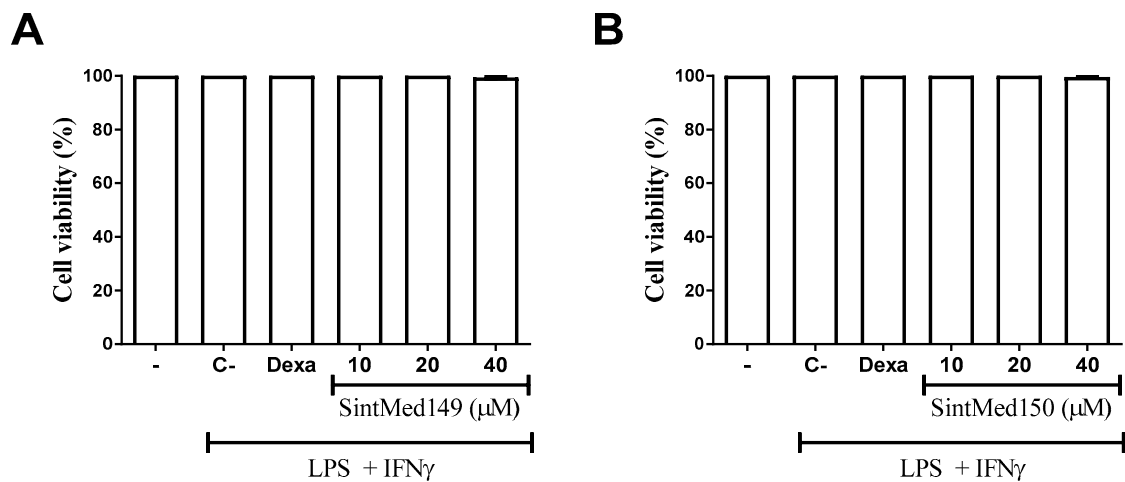


Figure 3. **SintMed149** and **SintMed150** did not affect peritoneal macrophage viability stimulated with LPS plus IFN γ . Mouse peritoneal exudate macrophages stimulated or not with LPS + IFN γ were cultured in the absence or presence of **SintMed149** (A) and **SintMed150** (B) (10, 20, and 40 μ M) or dexamethasone (Dexa; 40 μ M). Cell viability was determined by the Alamar Blue method. “-” refers to the group of untreated and unstimulated cells. C- refers to the group of untreated cells stimulated with LPS + IFN γ . Values represent the mean (\pm standard deviation) of four determinations obtained from three experiments performed.

Next, the anti-inflammatory effect of both compounds was better evaluated using a concentration-response curve in peritoneal macrophages. As expected, macrophage activation with LPS plus IFN γ increased the amount of nitrite production (Figure 4). Treatment with **SintMed149** and **SintMed150** inhibited, in a concentration-dependent manner, the production of nitrite ($p < 0.05$). Interestingly, the inhibitory effect of **SintMed149** and **SintMed150** was also observed in the production of the pro-inflammatory cytokines TNF and IL-1 β ($p < 0.05$) (Figure 5). Under the same conditions, dexamethasone, at a concentration of 10 μ M, also promoted the reduction of these cytokines and nitrite (Figures 4 and 5).

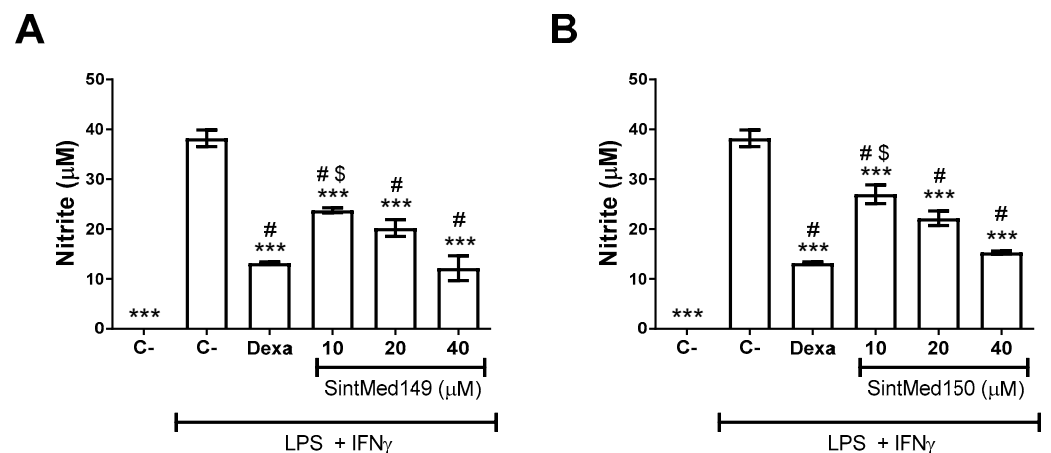


Figure 4. Ferrocenyl-*N*-acyl hydrazones **SintMed149** and **SintMed150** inhibit nitrite production by activated macrophages. Nitrite concentrations were determined in macrophage culture supernatants treated or not with hydrazones **SintMed149** (A) and **SintMed150** (B) (10, 20, and 40 μ M) or dexamethasone (Dexa; 10 μ M) in the presence of LPS (500 ng/mL) and IFN- γ (5 ng/mL). Values represent the mean (\pm standard deviation) of four determinations obtained in one of three experiments performed. *** $p < 0.001$ compared to untreated and LPS + IFN- γ -stimulated cultures. # $p < 0.05$ compared to untreated and unstimulated cultures with LPS + IFN- γ . \$ $p < 0.05$ compared to dexamethasone-treated and stimulated cultures.

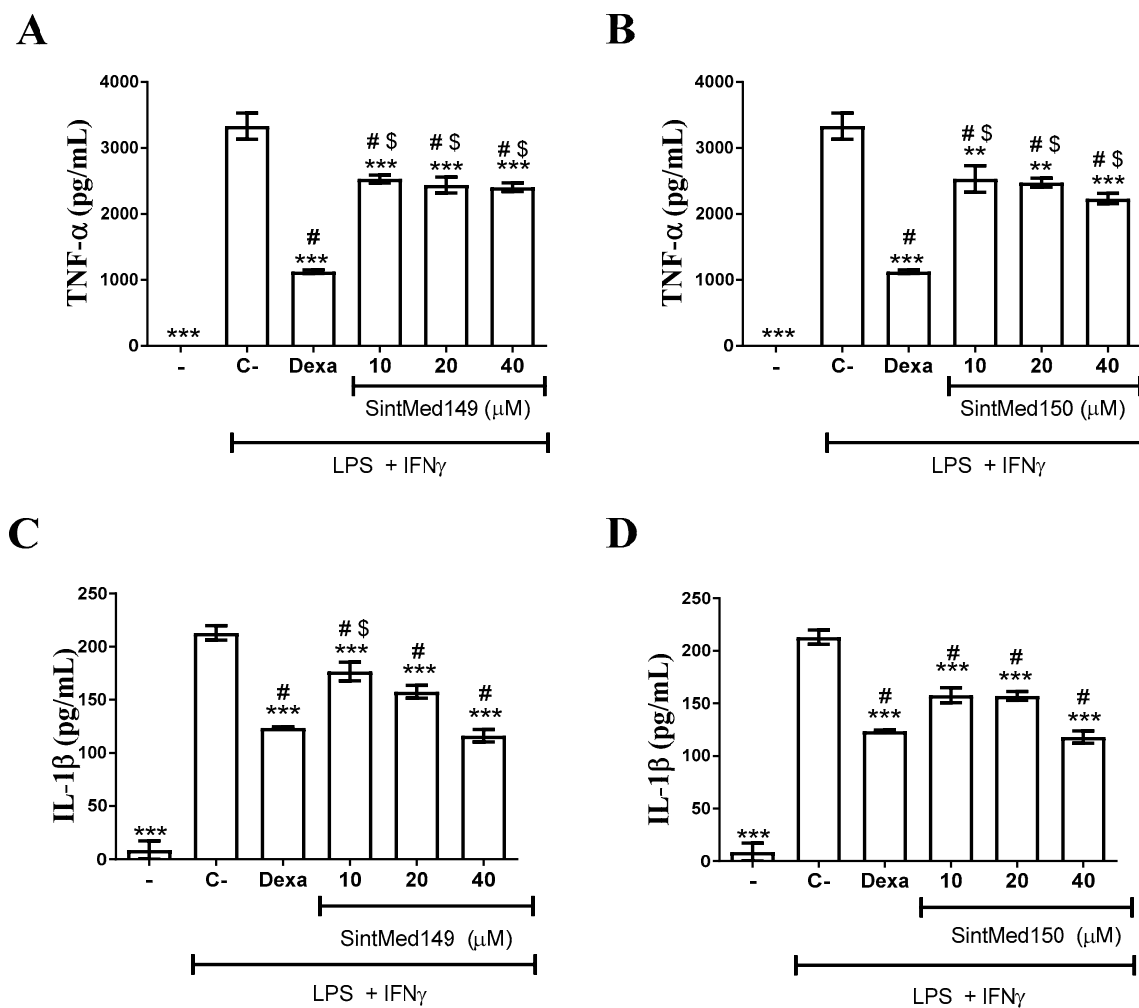


Figure 5. Assessment of cytokine production by peritoneal macrophages treated with **SintMed149** or **SintMed150**. Mouse peritoneal exudate macrophages stimulated or not with LPS + IFN- γ were cultured in the absence or presence of **SintMed149** (A,C) or **SintMed150** (B,D) (10, 20, and 40 μ M) or dexamethasone (Dexa; 10 μ M). Cell-free supernatants were collected after 4 h for TNF α quantification (A and B) or 24 h for IL-6 quantification (C and D). “-” refers to the group of untreated and unstimulated cells. C- refers to the group of untreated cells stimulated with LPS + IFN γ . Values represent the mean (\pm standard deviation) of four determinations obtained in one of three experiments performed. *** $p < 0.001$ compared to stimulated and untreated cells; ** $p < 0.01$ compared to stimulated and untreated cells; # $p < 0.05$ compared to unstimulated and untreated cells; \$ $p < 0.05$ compared to dexamethasone-treated cells.

To investigate the immunosuppressive activity of **SintMed149** and **SintMed150**, the levels of IL-2, IL-4, and IFN- γ were evaluated in the supernatant of cultures of splenocytes stimulated with concanavalin A. As shown in Figure 6, stimulation with concanavalin A induced a significant increase in the production levels of the cytokines IL-2, IL-4, and IFN- γ . Treatment using the hydrazones **SintMed149** and **SintMed150** promoted a significant and concentration-dependent reduction of IL-2 and **SintMed150** also performed the same feat in the production of IFN- γ . However, the molecules did not significantly reduce IL-4 levels. Under the same conditions, dexamethasone significantly reduced the levels of IL-2, IL-4, and IFN- γ (Figure 6).

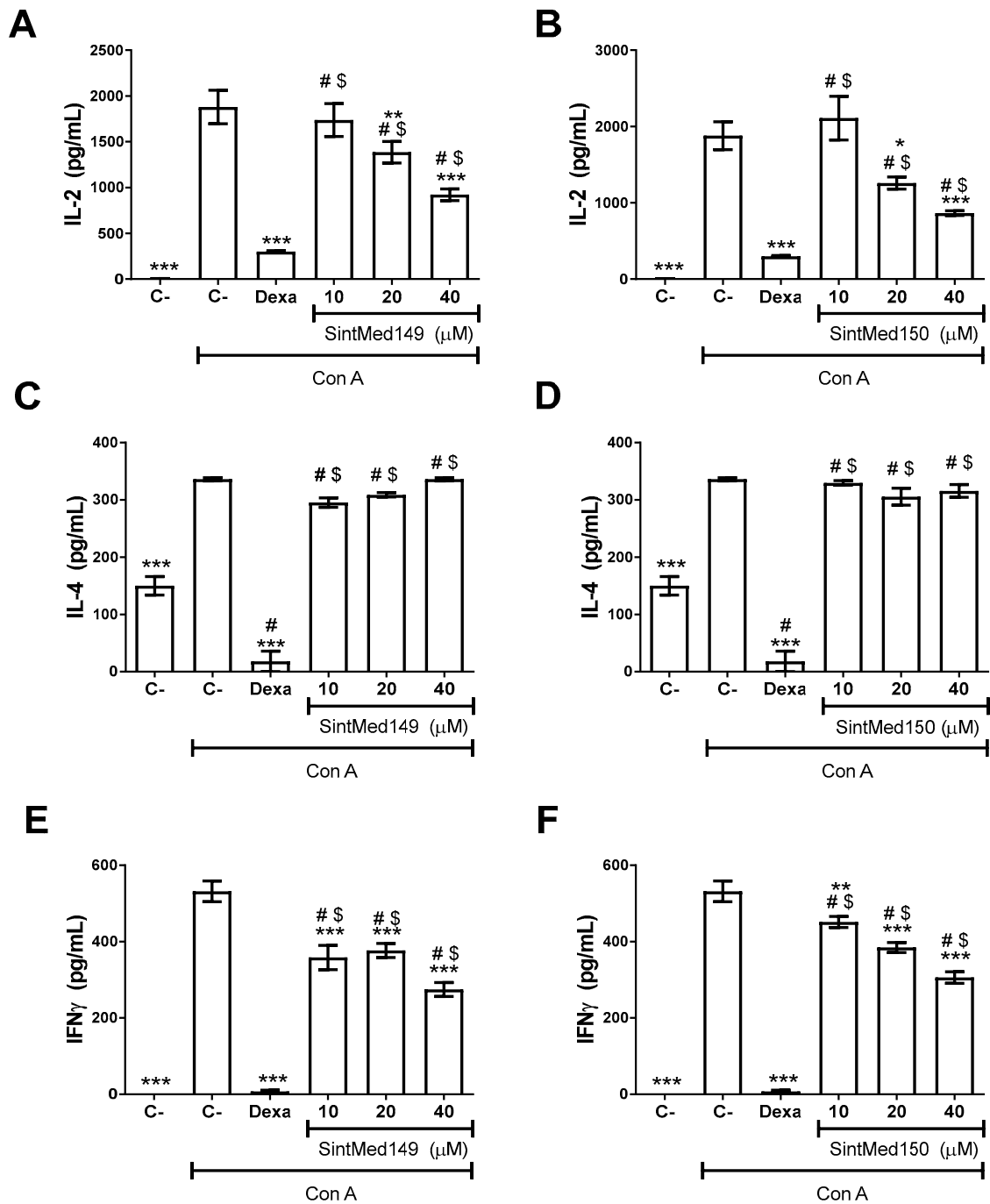


Figure 6. Assessment of cytokine production by splenocytes treated with **SintMed149** and **SintMed150**. The concentrations of IL-2 (A,B), IL-4 (C,D), and IFN- γ (E,F) were determined in cell-free supernatants from splenocyte cultures stimulated with concanavalin A (Con A, 5 μ g/mL) and treated or not with **SintMed149** and **SintMed150** (10, 20, 40 μ M) or dexamethasone (10 μ M) for 24 h. Culture supernatants were collected and cytokine quantification was performed by ELISA. Values represent the mean (\pm standard deviation) of four determinations obtained in one of three experiments performed. *** $p < 0.001$ compared to untreated and Con A-stimulated cultures ** $p < 0.01$ in comparison to untreated and Con A-stimulated cultures * $p < 0.05$ compared to untreated and Con A-stimulated cultures. # $p < 0.05$ compared to untreated and unstimulated cultures with Con A. \$ $p < 0.05$ compared to dexamethasone-treated and stimulated cultures.

After the *in vitro* results, we investigated the toxicity effect of a single dose of the compound **SintMed150** in BALB/c mice. Administration of 50 or 100 mg/kg of **SintMed150** did not cause mortality or the appearance of any sign of toxicity in animals (Table 2). In addition, no difference in body weight was observed in animals treated with **SintMed150** when compared to vehicle-treated mice (Table 3).

Table 2. Effect of **SintMed150** on behavioral and general appearance of male BALB/c mice.

Behavior and General Appearance	Observations		
	Vehicle	SintMed150 (50 mg/kg)	SintMed150 (100 mg/kg)
Changes in the eyes	No changes	No changes	No changes
Changes in the fur	No changes	No changes	No changes
Changes in the skin	No changes	No changes	No changes
Coma	Absent	Absent	Absent
Convulsions	Absent	Absent	Absent
Diarrhea	Absent	Absent	Absent
Lethargy	Absent	Absent	Absent
Salivation	Absent	Absent	Absent
Sleep	Usual	Usual	Usual
Tremors	Absent	Absent	Absent

The animals were observed daily for 14 days.

Table 3. Body weight of BALB/c mice treated with the compound **SintMed150**.

Days	Vehicle	SintMed150 (50 mg/kg)	SintMed150 (100 mg/kg)
0	21.6 (\pm 1.3)	20.9 (\pm 1.1)	20.1 (\pm 0.8)
7	21.8 (\pm 1.0)	21.1 (\pm 1.1)	20.4 (\pm 0.7)
14	22.3 (\pm 1.1)	21.7 (\pm 0.9)	21.0 (\pm 0.7)

Values represent the mean \pm standard deviation of six animals per group.

Then, we tested the compound **SintMed150** in a murine model of endotoxic shock induced by a lethal dose of LPS. As shown in Figure 7, in comparison with the vehicle group, the animals treated with the compound **SintMed150** had a longer survival time, despite, on the third day, all the animals treated with the dose of 50 mg/kg having already died. On the fourth day, only 20% of the group treated with the 100 mg/kg dose survived, this finding being statistically significant ($p < 0.05$). Under the same conditions, dexamethasone, at a dose of 25 mg/kg, promoted a more significant survival rate (83.3%).

Lastly, the anti-inflammatory effect of **SintMed150** was evaluated in a murine model of carrageenan-induced acute peritonitis. As can be seen in Figure 8, animals stimulated with carrageenan and treated with vehicle solution had a high number of neutrophils in the peritoneal lavage. Compared to the vehicle-treated group, pretreatment with **SintMed150** at 100 mg/kg caused a reduction in neutrophil migration of 44.6%. Under the same conditions, dexamethasone, at a dose of 25 mg/kg, induced a reduction of 55% in neutrophil migration (Figure 8).

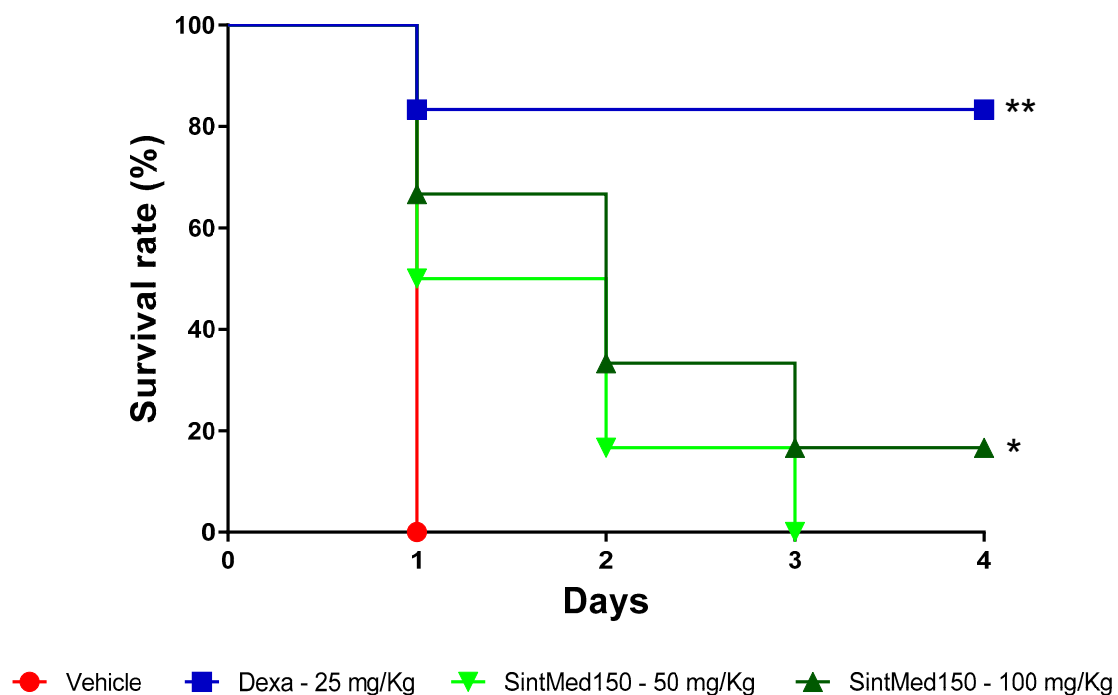


Figure 7. Survival curve of mice treated with **SintMed150** and submitted to endotoxic shock. Mice were orally treated with **SintMed150** at doses of 50 mg/kg (∇) and 100 mg/kg (\blacktriangle), or dexamethasone at a dose of 25 mg/kg (\blacksquare), or vehicle (\bullet). Survival was monitored for 4 days after LPS challenge. The results are from two experiments performed independently. * $p < 0.05$ compared to the vehicle group. ** $p < 0.01$ compared to the vehicle group. Statistical analysis was performed using Logrank (Mantel Cox).

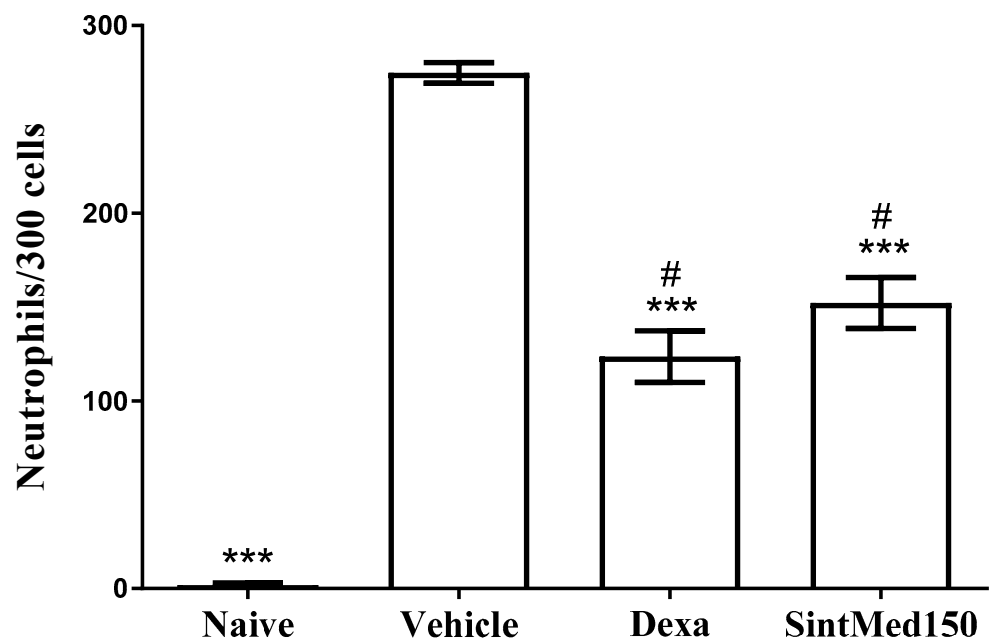


Figure 8. Effect of **SintMed150** in a carrageenan-induced model of acute peritonitis. BALB/c mice ($n = 5$ /group) were treated with **SintMed150** (100 mg/kg) or dexamethasone (Dexa; 25 mg/kg) or vehicle (solution containing 30% sorbitol, 10% Tween 80, and 60% saline) and challenged with 1% carrageenan solution. The naïve group consists of untreated and unchallenged animals. Values represent the means \pm S.D. of six mice/group. *** $p < 0.001$ compared to the vehicle group; # $p < 0.05$ compared to naïve group.

3. Discussion

The derivatives **SintMed**(141–156) were characterized by usual spectroscopic techniques, namely IR, ^1H NMR, and ^{13}C NMR, with structural assignments assisted by DEPT, HSQC, and HMQC experiments, confirming the structures and stereochemical features for each compound. ^1H NMR analysis of crude Fc-NAH derivatives has revealed that only the *E*-isomer was formed, in agreement with previously reported outcomes for other compounds synthesized using this method. In addition to the mild condition and low reaction time, cerium (III) chloride catalysis has proved to be highly stereoselective, leading exclusively to the *E*-isomers [31]. All compounds from this series exhibit a clear and easy pattern of signals in agreement with previously reported works, mainly based upon the analysis of the signals observed for the amidic ($-\text{CONH}-$) and iminic ($-\text{N}=\text{CH}-$) groups, which are singlets [29]. However, *N*-acyl hydrazones may exist as conformers due to the influence of some structural features of the substituents linked to the amidic carbonyl. It was ascertained that electron-withdrawing effects acting on an aromatic ring, *ortho*-substituents, or the linkage to non-aromatic substituents can destabilize the resonance effects involving the $-\text{CONH}-$ portion, favoring the possible emergence of rotamers. Signal duplication for Fc-NAH derivatives due to rotamery has been observed for the hydrogen atoms of the $-\text{CONH}-$ and $-\text{N}=\text{CH}-$ moieties and agreed with reported results from the literature [32,33]. Additionally, the Fc signals can also split due to the rotamery. The signal duplication does not follow a standard behavior, so different patterns can appear for different compounds, which are completely described in the Supplementary Materials. The crystal structure of compound **SintMed149** shows the *E*-configuration, confirming the stereochemical analysis based on NMR studies. It is also important to notice that this specific molecule is not planar throughout the aryl-*N*-acyl hydrazone backbone, corroborating the works of Lopes et al. [32] and da Silva et al. [33], which explain the nature of the rotamery observed for this compound (Supplementary Materials Figure S1). Any structural and/or electronic factors disrupting the resonance are at the origin of the rotamery observed for some members of the Fc-NAH series.

N-acyl hydrazones have been widely used in medicinal chemistry due to their ability to act on several molecular targets and ease of synthesis; therefore, the development of new NAH hybrids is an attractive strategy for drug design and discovery [34]. Several studies report the ability of NAH to modulate cells and inflammatory mediators of the immune response for in vitro and in vivo models of immune disorders [35,36]. The association with the ferrocene scaffold is a recognized strategy to enhance biological responses [37] and was expected to work well in our approach.

In this study, the immunomodulatory potential of 16 new Fc-NAH derivatives was investigated. The evaluated molecules presented non-cytotoxicity in the tested concentration, which reinforces the safety profile of the class, previously demonstrated in several cell lines, such as mouse splenocytes from BALB/c mice and J774 macrophages [11,13,38]. Meira et al. (2018) [13], using the same method described in this report, investigated the cytotoxicity of 24 *N*-acyl hydrazones and obtained CC_{50} values between 17.8 and >100 μM in the same cell line used in this report.

Knowing that nitric oxide (NO) is a key mediator of the inflammatory response, it is essential to verify the modulation of its production performed by the new compounds [39], as disclosed in Table 1. It was found that all tested Fc-NAH hybrids reduced the production of NO; however, some structural features seem to affect the activity, depending upon the aromatic moiety. **SintMed141** (phenyl) has exhibited 19.7% of NO inhibition production and was chosen as comparing parameter. Inspecting Table 1, only one compound has presented a poorer activity, namely derivative **SintMed146** (3,5-di-*t*-butyl-4-hydroxyphenyl) with an inhibition of 14.4%. The influence of the bulkiness of the *t*-butyl group on the biological response seems to be fundamental, especially in comparison to compounds **SintMed151** (3,4,5-trihydroxyphenyl) and **SintMed152** (3,4,5-trihydroxyphenyl), both similarly substituted but more active with 25.2% and 55.5% of inhibition, respectively. The substitution at the *meta* position of the phenyl ring reduces unequivocally the NO

production inhibition, as observed for compounds **SintMed153** (2-hydroxy-5-nitrophenyl, 43.7%) and **SintMed154** (3-chlorophenyl, 45.2%), both with activities lower than 50%. Heterocyclic aromatic rings such as in Fc-NAH hybrids **SintMed143** (2-furanyl) with 49.2% and **SintMed145** (2-quinoliny) with 49.6% and the ring-fused compound **SintMed155** (1-naphthyl) with 35.6% of NO inhibition suggest that this kind of substitution is related to moderate-to-poor biological responses. However, the *para* substitution at the phenyl ring seems to exert a positive effect on the inhibition of the NO production, as can be ascertained by compounds **SintMed144** (4-cyanophenyl, 55.2%) and **SintMed147** (4-trifluoromethylphenyl, 59.9%). A set of four molecules has disclosed the most important outcomes for the whole series. Bearing *ortho* substituents, compounds **SintMed142** (2-chlorophenyl, 49.3%), **SintMed148** (2-tolyl, 56.6%), **SintMed149** (2-bromophenyl, 71.7%), and **SintMed150** (2-phenoxyphenyl, 74.2%) have brought to light the importance of this substitution pattern to the enhancement of the biological response and suggested that the lipophilic character of the *ortho*-substituent is directly responsible for the inhibition of the NO production. The remarkable results found for **SintMed149** and **SintMed150** are higher than the control drug dexamethasone and arouse the interest of further investigation of their immunomodulatory profiles.

These data corroborate with previous investigations, in which *N*-acyl hydrazone derivatives have been shown to be effective in reducing nitric oxide production in macrophage cultures stimulated with LPS plus IFN- γ , at concentrations ranging from 2.5 to 30 μ M [11,13]. The previously studied compound **SintMed65**, derived from NAH and tested by Meira and collaborators (2018) [13], was able to decrease the levels of pro-inflammatory cytokines (TNF- α and IL-1 β) produced by macrophages during the inflammatory process. TNF- α is considered the “master regulator” of inflammatory responses, it is mainly produced by macrophages, and orchestrates the production of other inflammatory mediators, as well as macrophages and lymphocytes for injured tissues [40], while IL-1 β has potent pro-inflammatory activity and is crucial for the body’s defense against infections and injuries [41]. Here, it was observed that compounds **SintMed149** and **SintMed150** also promoted a significant reduction in TNF and IL-1 β production.

Evidence shows that the hydrazone fraction of the compounds has a pharmacophoric character for the inhibition of cyclooxygenase (COX) and that non-steroidal anti-inflammatory drugs containing the NAH fraction are less ulcerogenic [16,42]. The hydrazone derivative LaSSBio-1386 demonstrated the ability to inhibit the phosphorylation of the κ B protein, promoting a negative regulation of NF- κ B, a relevant inflammatory pathway, whose inhibition is related to the decrease in cytokine production and inflammatory response [11]. Other derivatives such as *N*-pyrazoloyl hydrazone of isatin and *N*-thiopheneacetyl hydrazone of isatin decreased the translocation of NF- κ B into the nucleus and suppressed the MAPK pathway, evidenced by a decrease in p-38, JNK, and ERK protein production, which interferes with the production of pro-inflammatory mediators [43]. In addition, compound 3a inhibited the activation of the TLR4 signaling pathway in macrophages that induces the activation of NF- κ B [44]. These findings encourage further investigations with NF- κ B and MAPK signaling pathways to understand the mechanism of action of ferrocene-*N*-acyl hydrazone.

Then, it was found that **SintMed149** and **SintMed150** decreased IL-2 and IFN- γ levels and neither of the two molecules reduced IL-4 levels. IL-2 promotes the growth, differentiation, and maturation of lymphocytes and IFN- γ promotes apoptosis in infected cells and activates macrophages and NK cells [45,46]. Moraes et al. (2018) [36] obtained similar results when investigating the anti-inflammatory potential of indole-*N*-acyl hydrazone derivatives in murine splenocyte cultures.

The endotoxic shock model was previously used by Guimarães and colleagues (2018) [13] to verify the survival of mice in the face of a lethal dose of LPS. Under the same conditions used in this study, the compound in question (LaSSBio-1386), at 50 and 100 mg/kg, promoted an animal survival of 50 and 85%, respectively. Previously, the anti-inflammatory activity of NAH derivatives from the inhibition of cell migration in murine models of the sub-

cutaneous air pocket and carrageenan-induced acute peritonitis was demonstrated [21,22]. The data presented here suggest that Fc-NAH molecules have the potential to modulate the immune response in inflammatory conditions.

4. Materials and Methods

4.1. Chemistry

All solvents and reactants were purchased from Sigma-Aldrich (Merck KGaA, Darmstadt, Germany), Fluka (Carvalhaes, Alvorada, RS, Brazil), Vetec (Vetec Química Fina, Duque de Caxias, RJ, Brazil), and Acros Chemicals (Thermo Fisher Scientific, Waltham, MA, USA), and were used without further purification. The reactions' progresses were monitored by thin-layer chromatography (TLC), performed onto glass-backed plates of silica gel 60 F254 with gypsum from Merck (Merck KGaA, Darmstadt, Germany), and all compounds were detected by ultraviolet light (254 nm). Melting points were determined with a capillary apparatus Gehaka PF 1500 Farma (Gehaka, São Paulo, SP, Brazil) and are uncorrected. NMR spectra were recorded at 400 MHz for hydrogen and 100 MHz for carbon, using a Varian UNMRS 400 spectrometer (Varian, Palo Alto, CA, USA), or at 300 MHz for hydrogen and 75 MHz for carbon nuclei, using a Varian Unitplus 300 NMR (Varian, Palo Alto, CA, USA). Analyses were determined in DMSO- d_6 with chemical shift values (δ) in parts per million (ppm) and coupling constants (J) in Hertz (Hz) and measured at 25 °C. ^1H and ^{13}C assignments were assisted by 2D experiments, such as DEPT full edit, HMBC, and HSQC. The description of the results was based on the IUPAC numbering and name recommendations. IR spectra were recorded on a Tensor27 FTIR spectrometer from Bruker (Bruker, Billerica, MA, USA) or a Spectrum 400 FTIR-FTNIR spectrometer from Perkin Elmer (Perkin Elmer, Waltham, MA, USA) with the samples being analyzed as KBr pellets. Elemental analyses were performed in a Perkin Elmer 2400 Series L elemental analyzer (Perkin Elmer, Waltham, MA, USA). All spectra are available in the Supplementary Materials section.

4.2. Preparation of Aryl Carboxylic Acids **2a–p** [30]

In a 100 mL round-bottom flask, 20 mmol of silver nitrate was suspended in 60 mL of potassium hydroxide aqueous solution (7%), which was stirred for 5 min before 10 mmol of the appropriate aldehydes **1a–p** was added into the suspension. The mixture was stirred at 60 °C for 1 h, then cooled to room temperature, and filtered. The filtrate was acidified with a hydrochloric acid solution (10%) until the formation of a precipitate, which was cooled in an ice bath, filtered out, and dried under vacuum. The crude products were characterized by comparing their melting points with literature values as well as by ^1H NMR analysis. Yields have ranged from 70 to 90%, and all solid products were directly used in the next step without further purification.

4.3. Preparation of Aryl Carboxylate Methyl Esters **3a–p** [29]

In a 100 mL round-bottomed flask, 6 mmol of crude carboxylic acids **2a–p** was placed with 30 mL of methanol. Then, 2 mL of concentrated sulfuric acid was added dropwise under vigorous stirring, and the solution was allowed to reflux overnight. After cooling to room temperature, the methanol was removed at a rotary evaporator to afford an oil, which was dissolved in ethyl acetate (30 mL), and extracted with saturated aqueous sodium carbonate (3×30 mL), followed by saturated sodium chloride (1×30 mL). The organic layer was dried over anhydrous sodium sulfate, filtered off, prior to solvent removal, and drying under vacuum to afford crude esters as oils or solids, in yields ranging from 80 to 95%. ^1H NMR data were found to agree with literature reports so that crude products could undergo the next reaction.

4.4. Preparation of Aryl Carbohydrazides **4a–p** [29]

In a 50 mL round-bottomed flask, 5 mmol of the corresponding methyl esters **3a–p** and 2 mL of ethanol were placed. Then, 2 mL of hydrazine hydrate (55%) was dropped

under stirring, and the solution was allowed to reflux overnight. After cooling to room temperature, the reaction mixture was placed in an ice bath and filtered to afford crude products as solids in yields from 70 to 90%. Based on ^1H NMR data and melting point measurements, the solid hydrazides could be reacted directly in the next step.

4.5. Preparation of Ferrocenyl-*N*-acyl Hydrazones **SintMed(141–156)**

To a stirred suspension of 1 mmol of appropriate hydrazide and 1 mmol of ferrocenecarboxaldehyde in 10 mL of methanol was added 10 mol-% cerium (III) chloride heptahydrate and the reaction mixture was stirred at 40 °C during 10–30 min. The reaction's completion was monitored by TLC. Once concluded, the heating was put away, and 10 mL of water was added to the medium. After standing at the refrigerator, vacuum filtration was carried out, and the solid was washed with cold water/ethanol 1:1 followed by cold water. ^1H NMR analysis of all crude products confirmed their purity and, in a few cases, residual methanol (δ 3.16 ppm) can be observed. Recrystallization from dioxane/water mixture afforded the pure products for biological purposes. Yields, melting points, and spectroscopic and elemental analysis data are listed below for each compound.

(*E*)-*N'*-(Ferrocenylmethylidene)benzohydrazide **SintMed141**: R_f 0.50 (AcOEt/Hexanes 1:1), red powder, 0.93 mmol, 93%, mp 178.8–180.5 °C (from dioxane/ H_2O 1:1); IR (KBr, ν_{max} cm^{-1}): 3441, 3226 (CONH), 3063 (Ar CH), 1646 (C=O), 1607 (C=C), 1557 (C=N); ^1H NMR (400 MHz; DMSO- d_6 , δH ppm): 11.5 (s, 1H, CONH), 8.29 (s, 1H, N=CH), 7.89 (d, 2H, $^3J = 6.9$ Hz, Ar H-2,6), 7.57 (d, 1H, $^3J = 6.8$ Hz, Ar H-4), 7.52 (d, 2H, $^3J = 6.8$ Hz, Ar H-3,5), 4.66 (s, 2H, N=CH-Cp H-2,5), 4.46 (s, 2H, N=CH-Cp H-3,4), 4.24 (s, 5H, Cp-H); ^{13}C NMR (100 MHz; DMSO- d_6 , δC ppm): 162.3 (1C, C=O), 149.0 (1C, N=CH), 133.6 (1C, Ar C-1), 131.3 (1C, Ar C-4), 128.3 (2C, Ar C-3,5), 127.4 (2C, Ar C-2,6), 78.8 (1C, N=CH-Cp C-1), 70.1 (2C, N=CH-Cp C-3,4), 68.9 (5C, Cp), 67.5 (2C, N=CH-Cp C-2,5); Anal Calcd for $\text{C}_{18}\text{H}_{16}\text{FeN}_2\text{O}$: C, 65.08; H, 4.86; N, 8.43; found: C, 65.01; H, 4.80; N, 8.51.

(*E*)-*N'*-(Ferrocenylmethylidene)-2-chlorobenzohydrazide **SintMed142**: R_f 0.56 (AcOEt/Hexanes 1:1), red powder, 0.91 mmol, 91%, mp 156.8–158.1 °C (from dioxane/ H_2O 1:1); IR (KBr, ν_{max} cm^{-1}): 3181 (CONH), 2993 (aliphatic CH), 1641 (C=O), 1598 (C=C), 1547 (C=N); ^1H NMR (400 MHz; DMSO- d_6 , δH ppm, $\approx 1.8:1$ rotamers mixture): 11.65 (s, CONH minor), 11.57 (s, 1H, CONH), 8.12 (s, 1H, N=CH), 7.88 (s, N=CH), 7.55–7.41 (m, 4H, Ar, and minor), 4.66 (s, 2H, N=CH-Cp H-2,5), 4.46 (s, 2H, N=CH-Cp H-3,4), 4.34 (s, N=CH-Cp H-2,5 minor), 4.31 (s, N=CH-Cp H-3,4 minor), 4.23 (s, 5H, Cp-H), 4.15 (s, Cp-H minor); ^{13}C NMR (100 MHz; DMSO- d_6 , δC ppm, $\approx 1.8:1$ rotamers mixture): 167.8 (CONH minor), 161.7 (1C, CONH), 149.1 (1C, N=CH), 144.5 (N=CH minor), 136.1 (Ar C-1 minor), 135.3 (1C, Ar C-1), 131.1, 130.3, 130.2, 129.8, 129.6, 129.2, 128.7, 128.5, 127.1, 126.7 (5C, Ar, and minor), 78.8 (N=CH-Cp C-1 minor), 78.5 (1C, N=CH-Cp C-1), 70.2 (2C, N=CH-Cp C-3,4), 69.7 (N=CH-Cp C-3,4 minor), 68.9 (5C, Cp), 68.8 (5C, Cp minor), 67.6 (2C, N=CH-Cp C-2,5), 67.1 (2C, N=CH-Cp C-2,5 minor); Anal Calcd for $\text{C}_{18}\text{H}_{15}\text{FeN}_2\text{ClO}$: C, 58.97; H, 4.12; N, 7.64; found: C, 58.86; H, 4.18; N, 7.54.

(*E*)-*N'*-(Ferrocenylmethylidene)furan-2-ylcarbohydrazide **SintMed143**: R_f 0.46 (AcOEt/Hexanes 1:1), dark-red powder, 0.91 mmol, 91%, mp 220.8–222.5 °C (from dioxane/ H_2O 1:1); IR (KBr, ν_{max} cm^{-1}): 3215 (CONH), 2925 (aliphatic CH), 1651 (C=O), 1606 (C=C); ^1H NMR (300 MHz; DMSO- d_6 , δH ppm): 11.5 (s, 1H, CONH), 8.28 (s, 1H, N=CH); 7.92 (s, 1H, Furyl H-5), 7.25 (s, 1H, Furyl H-3), 6.68 (s, 1H, Furyl H-4), 4.64 (s, 2H, N=CH-Cp H-2,5), 4.44 (s, 2H, N=CH-Cp H-3,4), 4.22 (s, 5H, Cp-H); ^{13}C NMR (75 MHz; DMSO- d_6 , δC ppm): 153.6 (1C, CONH), 149.1 (1C, N=CH), 146.8 (1C, Furyl C-2), 145.4 (1C, Furyl C-5), 114.3 (1C, Furyl C-3), 111.9 (1C, Furyl C-4), 78.7 (1C, N=CH-Cp C-1), 70.1 (2C, N=CH-Cp C-3,4), 68.9 (5C, Cp), 67.5 (2C, N=CH-Cp C-2,5); Anal Calcd for $\text{C}_{16}\text{H}_{14}\text{FeN}_2\text{O}_2$: C, 59.66; H, 4.38; N, 8.70; found: C, 59.57; H, 4.45; N, 8.78.

(*E*)-*N'*-(Ferrocenylmethylidene)-4-cyanobenzohydrazide **SintMed144**: R_f 0.50 (AcOEt/Hexanes 1:1), red powder, 0.98 mmol, 98%, mp 236.0–237.9 °C (from dioxane/ H_2O 1:1); IR (KBr, ν_{max} cm^{-1}): 3354, 3229 (CONH), 3090 (Ar CH), 2227 (C \equiv N), 1650 (C=O), 1611 (C=C), 1565 (C=N); ^1H NMR (300 MHz; DMSO- d_6 , δH ppm): 11.8 (s, 1H, CONH), 8.31 (s,

1H, N=CH), 8.05 (br s, 2H, Ar), 8.02 (br s, 2H, Ar), 4.67 (s, 2H, N=CH-Cp H-2,5), 4.45 (s, 2H, N=CH-Cp H-3,4), 4.22 (s, 5H, Cp-H); ¹³C NMR (75 MHz; DMSO-*d*₆, δC ppm): 160.9 (1C, CONH), 150.2 (1C, N=CH), 137.6 (1C, Ar C-1), 132.4 (2C, Ar), 128.3 (2C, Ar), 118.2 (1C, CN), 113.7 (1C, Ar C-4), 78.4 (1C, N=CH-Cp C-1), 70.3 (2C, N=CH-Cp C-3,4), 68.9 (5C, Cp), 67.6 (2C, N=CH-Cp C-2,5); Anal Calcd for C₁₉H₁₅FeN₃O: C, 63.89; H, 4.23; N, 11.76; found: C, 63.99; H, 4.18; N, 11.71.

(*E*)-*N'*-(Ferrocenylmethylidene)quinolin-2-ylcarbohydrazide **SintMed145**: *R*_f 0.66 (AcOEt/Hexanes 1:1), red powder, 0.91 mmol, 91%, mp 227.1–228.7 °C (from dioxane/H₂O 1:1); IR (KBr, ν_{max} cm⁻¹): 3238 (CONH), 3050 (Ar CH), 1664 (C=O), 1600 (C=C), 1533 (C=N); ¹H NMR (400 MHz; DMSO-*d*₆, δH ppm): 11.9 (s, 1H, CONH), 8.60 (d, 1H, ³*J* = 8.4 Hz, Quinoline H-4), 8.52 (s, 1H, N=CH), 8.21 (d, 1H, ³*J* = 8.0 Hz, Quinoline H-3), 8.20 (d, 1H, ³*J* = 8.0 Hz, Quinoline H-8), 8.11 (d, 1H, ³*J* = 8.4 Hz, Quinoline H-5), 7.92 (t, 1H, ³*J* = 7.2 Hz, Quinoline H-7), 7.75 (t, 1H, ³*J* = 7.6 Hz, Quinoline H-6), 4.69 (s, 2H, N=CH-Cp H-2,5), 4.48 (s, 2H, N=CH-Cp H-3,4), 4.27 (s, 5H, Cp-H); ¹³C NMR (100 MHz; DMSO-*d*₆, δC ppm): 159.7 (1C, C=O), 150.6 (1C, N=CH), 150.0 (1C, Quinoline C-2), 145.8 (1C, Quinoline C-8a), 137.9 (1C, Quinoline C-4), 130.5 (1C, Quinoline C-7), 129.1 (1C, Quinoline C-8), 128.8 (1C, Quinoline C-4a), 128.12 (1C, Quinoline C-5), 128.09 (1C, Quinoline C-6), 118.9 (1C, Quinoline C-3), 78.7 (1C, N=CH-Cp C-1), 70.2 (2C, N=CH-Cp C-3,4), 69.0 (5C, Cp), 67.6 (2C, N=CH-Cp C-2,5); Anal Calcd for C₂₁H₁₇FeN₃O: C, 65.82; H, 4.47; N, 10.96; found: C, 65.75; H, 4.52; N, 11.03.

(*E*)-*N'*-(Ferrocenylmethylidene)-3,5-*tert*-butyl-4-hydroxybenzohydrazide **SintMed146**: *R*_f 0.76 (AcOEt/Hexanes 1:1), red powder, 0.97 mmol, 97%, mp 256.2–258.4 °C (dec, from dioxane/H₂O 1:1); IR (KBr, ν_{max} cm⁻¹): 3627, 3610 (br OH), 3507, 3223 (CONH), 3082 (Ar CH), 2912 (aliphatic CH), 1640 (C=O), 1607 (C=C), 1556 (C=N); ¹H NMR (400 MHz; DMSO-*d*₆, δH ppm): 11.3 (s, 1H, CONH), 8.29 (s, 1H, N=CH), 7.63 (s, 3H, OH, and Ar H-2,6), 4.64 (s, 2H, N=CH-Cp H-2,5), 4.43 (s, 2H, N=CH-Cp H-3,4), 4.22 (s, 5H, Cp-H), 1.42 (s, 18H, 2*x*^tBu); ¹³C NMR (100 MHz; DMSO-*d*₆, δC ppm): 163.3 (1C, C=O), 156.9 (1C, Ar C-4), 148.2 (1C, N=CH), 138.3 (2C, Ar C-3,5), 124.8 (1C, Ar C-1), 124.2 (2C, Ar C-2,6), 79.2 (1C, N=CH-Cp C-1), 69.9 (2C, N=CH-Cp C-3,4), 68.9 (5C, Cp), 67.4 (2C, N=CH-Cp C-2,5), 34.5 (2C, C^tBu), 30.1 (6C, C^tBu); Anal Calcd for C₂₆H₃₂FeN₂O₂: C, 67.83; H, 7.01; N, 6.08; found: C, 67.89; H, 6.94; N, 6.13.

(*E*)-*N'*-(Ferrocenylmethylidene)-4-(trifluoromethyl)benzohydrazide **SintMed147**: *R*_f 0.74 (AcOEt/Hexanes 1:1), red powder, 0.99 mmol, 99%, mp 220.9–222.5 °C (from dioxane/H₂O 1:1); IR (KBr, ν_{max} cm⁻¹): 3355, 3201 (CONH), 3083, 3053 (Ar CH), 1657 (C=O), 1608 (C=C), 1564 (C=N); ¹H NMR (400 MHz; DMSO-*d*₆, δH ppm): 11.7 (s, 1H, CONH), 8.32 (s, 1H, N=CH), 8.10 (d, 2H, ³*J* = 5.2 Hz, Ar H-2,6), 7.90 (d, 2H, ³*J* = 6.0 Hz, Ar H-3,5), 4.68 (s, 2H, N=CH-Cp H-2,5), 4.47 (s, 2H, N=CH-Cp H-3,4), 4.24 (s, 5H, Cp-H); ¹³C NMR (100 MHz; DMSO-*d*₆, δC ppm): 161.1 (1C, C=O), 150.0 (1C, N=CH), 137.4 (1C, Ar C-1), 131.3 (q, 1C, ²*J*_{FC} = 31 Hz, Ar C-4), 128.3 (2C, Ar C-2,6), 125.3 (2C, Ar C-3,5), 126.1 (q, 1C, ¹*J*_{FC} = 200 Hz, CF₃), 78.5 (1C, N=CH-Cp C-1), 70.2 (2C, N=CH-Cp C-3,4), 68.9 (5C, Cp), 67.6 (2C, N=CH-Cp C-2,5); ¹⁹F NMR (376 MHz; DMSO-*d*₆, δF ppm): -61.2 (s, 1F, CF₃); Anal Calcd for C₁₉H₁₅FeN₂F₃O: C, 57.03; H, 3.78; N, 7.00; found: C, 56.99; H, 3.83; N, 7.03.

(*E*)-*N'*-(Ferrocenylmethylidene)-2-methylbenzohydrazide **SintMed148**: *R*_f 0.55 (AcOEt/Hexanes 1:1), red powder, 0.93 mmol, 93%, mp 207.9–209.8 °C (from dioxane/H₂O 1:1); IR (KBr, ν_{max} cm⁻¹): 3174 (CONH), 3056 (Ar CH), 2991 (aliphatic CH), 1643 (C=O), 1600 (C=C), 1559 (C=N); ¹H NMR (400 MHz; DMSO-*d*₆, δH ppm, ≈7:3 rotamers mixture): 11.4 (s, 1H, CONH, and minor), 8.15 (s, 1H, N=CH), 7.89 (s, N=CH minor), 7.43–7.29 (m, 4H, Ar H-3,4,5,6, and minor), 4.64 (s, 2H, N=CH-Cp H-2,5), 4.44 (s, 2H, N=CH-Cp H-3,4), 4.36 (s, N=CH-Cp H-2,5 minor), 4.31 (s, N=CH-Cp H-3,4 minor), 4.23 (s, 5H, Cp-H), 4.17 (s, Cp-H minor), 2.38 (s, 3H, CH₃), 2.30 (s, CH₃ minor); ¹³C NMR (100 MHz; DMSO-*d*₆, δC ppm, ≈7:3 rotamers mixture): 170.5 (CONH minor), 164.4 (1C, CONH), 148.4 (1C, N=CH), 144.0 (N=CH minor), 136.1, 135.6, 135.4, 134.4, 130.4, 129.6, 129.4, 128.7, 127.24, 127.17, 125.4, 124.9 (6C, Ar, and minor), 78.9 (N=CH-Cp C-1 minor), 78.8 (1C, N=CH-Cp C-1), 70.0 (2C, N=CH-Cp C-3,4), 69.6 (N=CH-Cp C-3,4 minor), 68.8 (5C, Cp), 68.7 (Cp minor), 67.4 (2C,

N=CH-Cp C-2,5), 67.0 (N=CH-Cp C-2,5 minor), 19.23 (CH₃ minor), 19.18 (1C, CH₃); Anal Calcd for C₁₉H₁₈FeN₂O: C, 65.92; H, 5.24; N, 8.09; found: C, 65.99; H, 5.20; N, 8.15.

(*E*)-*N'*-(Ferrocenylmethylidene)-2-bromobenzohydrazide **SintMed149**: *R*_f 0.70 (AcOEt/Hexanes 1:1), red powder, 0.87 mmol, 87%, mp 163.4–165.8 °C (dec, from dioxane/H₂O 1:1); IR (KBr, ν_{\max} cm⁻¹): 3190 (CONH), 3055 (Ar CH), 1656 (C=O), 1600 (C=C), 1562 (C=N); ¹H NMR (400 MHz; DMSO-*d*₆, δ H ppm, \approx 2:1 rotamers mixture): 11.6 (s, CONH minor), 11.5 (s, 1H, CONH), 8.11 (s, 1H, N=CH), 7.87 (s, N=CH minor), 7.71 (d, 1H, ³*J* = 8.0 Hz, Ar H-6), 7.68 (d, ³*J* = 8.0 Hz, Ar H-6 minor), 7.54–7.37 (m, 3H, Ar H-3,4,5, and minor), 4.66 (s, 2H, N=CH-Cp H-2,5), 4.46 (s, 2H, ³*J* = 2.8 Hz, N=CH-Cp H-3,4), 4.34 (s, N=CH-Cp H-2,5 minor), 4.31 (s, N=CH-Cp H-3,4 minor), 4.24 (s, 5H, Cp-H), 4.16 (s, Cp-H minor); ¹³C NMR (100 MHz; DMSO-*d*₆, δ C ppm): 162.5 (1C, CONH), 149.0 (1C, N=CH), 144.4 (N=CH minor), 137.5, 132.7, 131.9, 131.2, 130.2, 129.2, 128.5, 127.6, 127.1 (5C, Ar C-1,3,4,5,6, and minor), 119.4 (1C, Ar C-2), 78.9 (N=CH-Cp C-1 minor), 78.6 (1C, N=CH-Cp C-1), 70.2 (2C, N=CH-Cp C-3,4), 69.7 (N=CH-Cp C-3,4 minor), 68.91 (5C, Cp), 68.86 (Cp minor), 67.6 (2C, N=CH-Cp C-2,5), 67.1 (N=CH-Cp C-2,5 minor); Anal Calcd for C₁₈H₁₅FeN₂BrO: C, 52.59; H, 3.68; N, 6.81; found: C, 52.52; H, 3.71; N, 6.90.

(*E*)-*N'*-(Ferrocenylmethylidene)-2-phenoxybenzohydrazide **SintMed150**: *R*_f 0.65 (AcOEt/Hexanes 1:1), red powder, 0.83 mmol, 83%, mp 177.9–179.5 °C (dec, from dioxane/H₂O 1:1); IR (KBr, ν_{\max} cm⁻¹): 3308 (CONH), 3060 (Ar CH), 1661 (C=O), 1602 (C=C), 1541 (C=N); ¹H NMR (400 MHz; DMSO-*d*₆, δ H ppm, \approx 7:3 rotamers mixture): 11.45 (s, CONH minor), 11.38 (s, 1H, CONH), 8.14 (s, 1H, N=CH), 7.84 (s, N=CH minor), 7.67–6.98 (m, 9H, Ar and OPh, and minor), 4.62 (s, 2H, N=CH-Cp H-2,5), 4.42 (s, 2H, N=CH-Cp H-3,4), 4.39 (s, N=CH-Cp H-2,5 minor), 4.32 (s, N=CH-Cp H-3,4 minor), 4.20 (s, 5H, Cp-H), 4.12 (s, Cp-H minor); ¹³C NMR (100 MHz; DMSO-*d*₆, δ C ppm, \approx 7:3 rotamers mixture): 167.9 (CONH minor), 161.1 (1C, CONH), 156.5, 153.0 (2C, Ar), 148.4 (1C, N=CH), 144.2 (N=CH minor), 131.7, 130.4, 130.2, 129.8, 129.6, 128.8, 128.6, 127.5, 123.6, 123.4, 123.1, 122.9, 120.1, 119.1, 118.4, 118.3, 118.0 (10C, Ar, OPh, and minor), 78.9 (N=CH-Cp C-1 minor), 78.7 (1C, N=CH-Cp C-1), 70.1 (2C, N=CH-Cp C-3,4), 69.7 (N=CH-Cp C-3,4 minor), 68.8 (5C, Cp), 68.7 (Cp minor), 67.5 (2C, N=CH-Cp C-2,5), 67.1 (N=CH-Cp C-2,5 minor); Anal Calcd for C₂₄H₂₀FeN₂O₂: C, 67.94; H, 4.75; N, 6.60; found: C, 67.87; H, 4.82; N, 6.65.

(*E*)-*N'*-(Ferrocenylmethylidene)-3,4,5-trihydroxybenzohydrazide **SintMed151**: *R*_f 0.10 (AcOEt), red powder, 0.96 mmol, 96%, mp 305.3–306.0 °C (dec, from dioxane/H₂O 1:1); IR (KBr, ν_{\max} cm⁻¹): 3552–3000 (br, OH), 3225 (CONH), 3084 (Ar CH), 1633 (C=O), 1608 (C=C), 1570 (C=N); ¹H NMR (300 MHz; DMSO-*d*₆, δ H ppm): 11.2 (s, 1H, CONH), 9.13 (s, 2H, 3,5-OH), 8.77 (s, 1H, 4-OH), 8.23 (s, 1H, N=CH), 6.90 (s, 2H, Ar H-2,6), 4.62 (s, 2H, N=CH-Cp H-2,5), 4.42 (s, 2H, N=CH-Cp H-3,4), 4.21 (s, 5H, Cp-H); ¹³C NMR (75 MHz; DMSO-*d*₆, δ C ppm): 162.5 (1C, C=O), 147.8 (1C, N=CH), 145.4 (2C, Ar C-3,5), 136.6 (1C, Ar C-4), 123.6 (1C, Ar C-1), 106.9 (2C, Ar C-2,6), 79.2 (1C, N=CH-Cp C-1), 69.9 (2C, N=CH-Cp C-3,4), 68.9 (5C, Cp), 67.4 (2C, N=CH-Cp C-2,5); Anal Calcd for C₁₈H₁₆FeN₂O₄: C, 56.87; H, 4.24; N, 7.37; found: C, 56.82; H, 4.31; N, 7.32.

(*E*)-*N'*-(Ferrocenylmethylidene)-3,4,5-trimethoxybenzohydrazide **SintMed152**: *R*_f 0.18 (AcOEt/Hexanes 1:1), red powder, 0.90 mmol, 90%, mp 237.8–239.5 °C (dec, from dioxane/H₂O 1:1); IR (KBr, ν_{\max} cm⁻¹): 3235 (CONH), 3083 (Ar CH), 2942 (aliphatic CH), 1646 (C=O), 1608 (C=C), 1582 (C=N); ¹H NMR (400 MHz, DMSO-*d*₆, δ H ppm): 11.4 (s, 1H, CONH), 8.32 (s, 1H, N=CH), 7.23 (s, 2H, Ar H-2,6), 4.66 (s, 2H, N=CH-Cp H-2,5), 4.45 (s, 2H, N=CH-Cp H-3,4), 4.23 (s, 5H, Cp-H), 3.86 (s, 6H, 3,5-OCH₃), 3.73 (s, 3H, 4-OCH₃); ¹³C NMR (100 MHz, DMSO-*d*₆, δ C ppm): 161.8 (1C, C=O), 152.6 (2C, Ar C-3,5), 149.1 (1C, N=CH), 140.2 (1C, Ar C-4), 128.7 (1C, Ar C-1), 105.0 (2C, Ar C-2,6), 78.8 (1C, N=CH-Cp C-1), 70.1 (2C, N=CH-Cp C-3,4), 68.9 (5C, Cp), 67.5 (2C, N=CH-Cp C-2,5), 60.0 (1C, 4-OCH₃), (2C, 3,5-OCH₃); Anal Calcd for C₂₁H₂₂FeN₂O₄: C, 59.73; H, 5.25; N, 6.63; found: C, 59.65; H, 5.22; N, 6.70.

(*E*)-*N'*-(Ferrocenylmethylidene)-3,4,5-trimethoxybenzohydrazide **SintMed153**: *R*_f 0.18 (AcOEt/Hexanes 1:1), yellow powder, yield 86%, mp 221.4–222.6 °C (dec, from dioxane/H₂O 1:1); IR (KBr, ν_{\max} cm⁻¹): 3379, 3328, 3255 (CONH, OH), 3095 (Ar CH), 1630 (C=O), 1558 (C=N); ¹H NMR (400 MHz; DMSO-*d*₆, δ H ppm, \approx 2:1 rotamers mixture): 13.6 (s, 1H,

CONH), 9.23 (s, 1H, Ar H-6), 9.11 (s, Ar H-6 minor), 8.37 and 8.35 (2s, 1H, Ar H-4 major and minor), 8.12 (s, 1H, N=CH), 7.34 (s, 1H, Ar H-3), 4.50 (s, 2H, N=CH-Cp H-2,5), 4.38 (s, 2H, N=CH-Cp H-3,4), 4.16 (s, 5H, Cp-H); ^{13}C NMR (100 MHz; DMSO- d_6 , δC ppm): 167.1 (1C, CONH), 149.0 (1C, N=CH), 136.1 (1C, Ar C-2), 134.4 (1C, Ar C-5), 128.1 (1C, Ar C-4), 127.4 (1C, Ar C-6), 126.3 (1C, Ar C-1), 120.9 (1C, Ar C-3), 78.7 (1C, N=CH-Cp C-1), 69.9 (2C, N=CH-Cp C-3,4), 68.8 (5C, Cp), 67.5 (2C, N=CH-Cp C-2,5); Anal Calcd for $\text{C}_{18}\text{H}_{15}\text{FeN}_3\text{O}_4$: C, 54.99; H, 3.85; N, 10.69; found: C, 54.92; H, 3.84; N, 10.74.

(*E*)-*N'*-(Ferrocenylmethylidene)-3-chlorobenzohydrazide **SintMed154**: R_f 0.53 (AcOEt/Hexanes 3:7), red powder, yield 98%, mp 225.7–228.2 °C (dec, from dioxane/ H_2O 1:1); IR (KBr, ν_{max} cm^{-1}): 3196 (CONH), 3063 (Ar CH), 1643 (C=O), 1608 (C=C), 1568 (C=N); ^1H NMR (400 MHz, DMSO- d_6 , δH ppm): 11.6 (s, 1H, CONH), 8.29 (s, 1H, N=CH), 7.95 (s, 1H, Ar H-2), 7.86 (d, 1H, $^3J = 6.8$ Hz, Ar H-6), 7.65 (d, 1H, $^3J = 7.6$ Hz, Ar H-4), 7.55 (t, 1H, $^3J = 7.6$ Hz, Ar H-5), 4.67 (s, 2H, N=CH-Cp H-2,5), 4.46 (s, 2H, N=CH-Cp H-3,4), 4.23 (s, 5H, Cp); ^{13}C NMR (100 MHz, DMSO- d_6 , δC ppm): 160.8 (C=O), 149.7 (N=CH), 135.6 (1C, Ar C-3), 133.1 (1C, Ar C-1), 131.2 (1C, Ar C-4), 130.3 (1C, Ar C-5), 127.1 (1C, Ar C-2), 126.2 (1C, Ar C-6), 78.6 (1C, N=CH-Cp C-1), 70.2 (2C, N=CH-Cp C-3,4), 68.9 (5C, Cp), 67.5 (2C, N=CH-Cp C-2,5); Anal Calcd for $\text{C}_{18}\text{H}_{15}\text{FeN}_2\text{ClO}$: C, 58.97; H, 4.12; N, 7.64; found: C, 59.04; H, 4.09; N, 7.58.

(*E*)-*N'*-(Ferrocenylmethylidene)-1-naphtylcarbohydrazide **SintMed155**: R_f 0.68 (AcOEt/Hexanes 1:1), red powder, yield 93%, mp 233.0–234.4 °C (dec, from dioxane/ H_2O 1:1); IR (KBr, ν_{max} cm^{-1}): 3185 (CONH), 3035 (Ar CH), 2977, 2845 (aliphatic CH), 1636 (C=O), 1617 (C=C), 1564 (C=N); ^1H NMR (400 MHz; DMSO- d_6 , δH ppm): 11.7 (s, 1H, CONH), 8.24–8.22 (m, 1H, Naphtyl), 8.20 (s, 1H, N=CH), 8.08 (d, 1H, $^3J = 8.0$ Hz, Naphtyl), 8.03–8.00 (m, 1H, Naphtyl), 7.74 (d, 1H, $^3J = 7.2$ Hz, Naphtyl), 7.61–7.58 (m, 3H, Naphtyl), 4.68 (s, 2H, N=CH-Cp H-2,5), 4.47 (s, 2H, N=CH-Cp H-3,4), 4.26 (s, 5H, Cp-H); ^{13}C NMR (100 MHz; DMSO- d_6 , δC ppm): 163.9 (C=O), 148.9 (N=CH), 133.1, 133.0, 130.2, 130.0, 128.2, 126.8, 126.3, 125.6, 125.1, 124.9 (10C, Naphtyl), 78.8 (1C, N=CH-Cp C-1), 70.1 (2C, N=CH-Cp C-3,4), 68.9 (5C, Cp), 67.5 (2C, N=CH-Cp C-2,5); Anal Calcd for $\text{C}_{22}\text{H}_{18}\text{FeN}_2\text{O}$: C, 69.13; H, 4.75; N, 7.33; found: C, 69.21; H, 4.73; N, 7.36.

(*E*)-*N'*-(Ferrocenylmethylidene)-2,4-dimethoxybenzohydrazide **SintMed156**: R_f 0.32 (AcOEt/Hexanes 1:1), red powder, yield 87%, mp 123.9–126.6 °C (dec, from dioxane/ H_2O 1:1); IR (KBr, ν_{max} cm^{-1}): 3223 (CONH), 3083 (Ar CH), 2836 (aliphatic CH), 1641 (C=O), 1603 (C=C), 1561 (C=N); ^1H NMR (400 MHz; DMSO- d_6 , δH ppm): 11.4 (s, 1H, CONH), 8.30 (s, 1H, N=CH), 7.55 (d, 1H, $^3J = 8.0$ Hz, Ar H-5), 7.48 (s, 1H, Ar H-3), 7.07 (d, 1H, $^3J = 8.8$ Hz, Ar H-6), 4.65 (s, 2H, N=CH-Cp H-2,5), 4.44 (s, 2H, N=CH-Cp H-3,4), 4.23 (s, 5H, Cp-H), 3.84 (s, 3H, OCH_3), 3.83 (s, 3H, OCH_3); ^{13}C NMR (100 MHz; DMSO- d_6 , δC ppm): 161.8 (C=O), 151.4 (1C, Ar C-4), 148.5 (1C, Ar C-2), 148.2 (N=CH), 125.6 (Ar C-1), 120.7 (1C, Ar C-5), 110.9 (1C, Ar C-6), 110.7 (1C, Ar C-3), 79.0 (1C, N=CH-Cp C-1), 70.0 (2C, N=CH-Cp C-3,4), 68.9 (5C, Cp), 67.4 (2C, N=CH-Cp C-2,5), 55.5 (2C, 2x OCH_3); Anal Calcd for $\text{C}_{20}\text{H}_{20}\text{FeN}_2\text{O}_3$: C, 61.24; H, 5.14; N, 7.14; found: C, 61.16; H, 5.15; N, 7.09.

4.6. X-ray Crystallographic Analysis

Single crystals of compound **SintMed149** were grown by slow evaporation of an acetone/dichloromethane (1:1) solution. The X-ray diffraction experiment was performed at 100 K on a Rigaku Synergy-S diffractometer (Applied Rigaku Technologies, Inc., Austin, TX, USA) with Mo $K\alpha$ radiation ($\lambda = 0.71073$ Å). The CrysAlisPro 1.171.42.67a program (CrysAlisPRO, Oxford Diffraction / Agilent Technologies UK Ltd., Yarnton, UK) was used for data collection, cell refinement, data reduction, and gaussian method absorption correction. The structure was solved and refined using the software SHELXT2015 [47] and refined by SHELXL2015 [48] hosted on the OLEX2 program [49]. All atoms, except hydrogen, were identified and refined by least-squares full matrix F^2 with anisotropic thermal parameters. The crystallographic tables and the structure representations were generated by OLEX2. Details of the single-crystal X-ray diffraction experiment can be found

in the Supplementary Materials as well as on the CCDC database (www.ccdc.cam.ac.uk/, accessed on 12 September 2022) free of charge under deposit number 2214776.

4.7. Drugs

Dexamethasone (Sigma-Aldrich, St Louis, MO, USA), a synthetic glucocorticoid, was used as a positive control in immunomodulatory assays. Gentian violet (Synth, São Paulo, SP, Brazil) was used as a positive control in the cytotoxicity assays. All compounds were solubilized in dimethylsulfoxide (DMSO; PanReac, Barcelona, Spain) and diluted in Dulbecco's modified Eagle medium (DMEM; Life Technologies, GIBCO-BRL; Waltham, MA, USA) for use in the in vitro assays. The final concentration of DMSO was less than 0.1% in all in vitro experiments. For in vivo assays, the compounds were solubilized in a solution containing 30% sorbitol (Sigma-Aldrich), 10% Tween 80 (Sigma-Aldrich), and 60% saline.

4.8. Animals

Male BALB/c mice, aged between 4–8 weeks, were provided by the animal breeding facility of Gonçalo Moniz Institute, Salvador, Brazil, and maintained in sterilized cages with controlled temperature (22 ± 2 °C) and humidity ($55 \pm 10\%$), water ad libitum, and receiving a balanced diet for rodent. The experiments and procedures with animals were approved by the institution's committee on the ethical handling of laboratory animals (approved number: L-IGM-018/15).

4.9. Cytotoxicity to Mammalian Cells

J774 macrophages were seeded into 96-well plates at a cell density of 1×10^4 cells/well in a DMEM medium supplemented with 10% fetal bovine serum (FBS; GIBCO) and 50 µg/mL of gentamicin (Life Technologies, Carlsbad, CA, USA) and incubated for 24 h at 37 °C and 5% CO₂. After that time, each compound was added in six concentrations (50–1.56 µM), in triplicate, and incubated for 72 h. At the end of treatment, 20 µL/well of Alamar Blue (Invitrogen) was added to the plates for 4 h. using a SpectraMax 190 Microplate Reader (Molecular Devices, Sunnyvale, CA, USA).

As a positive control, gentian violet was used at concentrations ranging from 0.04 to 10 µM. CC₅₀ values were calculated using data from three independent experiments.

The second set of experiments was performed using peritoneal macrophages activated with LPS (500 ng/mL, Sigma-Aldrich) and IFN γ (5 ng/mL; Sigma-Aldrich).

Peritoneal exudate macrophages were obtained by washing, with a cold DMEM medium, the peritoneal cavity of BALB/c mice 4–5 days after injection of 3% thioglycolate (Sigma-Aldrich) in saline (1.5 mL per mouse). Cells were seeded into 96-well plates at a cell density of 1×10^5 cells/well in a DMEM medium supplemented with 10% FBS and 50 µg/mL of gentamicin and incubated for 24 h at 37 °C and 5% CO₂. After that time, each sample was added (12.5, 25, and 50 µM), in triplicate and incubated for 72 h. At the end of treatment, 20 µL/well of Alamar Blue (Invitrogen) were added to the plates for 10 h. Colorimetric readings were performed at 570 and 600 nm using a SpectraMax 190 Microplate Reader (Molecular Devices, Sunnyvale, CA, USA).

4.10. Macrophage Cultures

Immortalized J774 macrophages (2×10^5 cells/well) or peritoneal macrophages (2×10^5 cells/well) were incubated in 96-well plates in a DMEM medium supplemented with 10% FBS and 50 µg/mL of gentamicin, in triplicate, stimulated or not with LPS (500 ng/mL) and IFN- γ (5 ng/mL), and treated or not with different concentrations of the evaluated ferrocenyl-*N*-acyl hydrazones. The cells were incubated for 4 or 24 h at 37 °C and 5% CO₂. Cell-free supernatants were collected after 4 h (for TNF α measurement) and 24 h (for IL-1 β , TNF α , and nitrite quantifications), and kept at -80 °C until use.

4.11. Splenocyte Cultures

BALB/c splenocyte suspensions were prepared in a DMEM medium supplemented with FBS and gentamicin. Splenocytes (5×10^6 cells/well) were plated in 24-well plates, in triplicate, and stimulated or not with concanavalin A (Con A; $5 \mu\text{g}/\text{mL}$, Sigma-Aldrich). To evaluate lymphocyte function, splenocytes were activated in the absence or presence of various concentrations of **SintMed149** and **SintMed150** (10, 20, and $40 \mu\text{M}$). After 24 h of treatment, cell-free supernatants were collected and kept at -80°C until use.

4.12. Assessment of Cytokine and Nitric Oxide Production

The dosage of cytokines IFN- γ , IL-1 β , IL-2, IL-4, and TNF α was performed from the supernatant of peritoneal macrophages or splenocytes were determined by enzyme-linked immunosorbent assay (ELISA), using DuoSet kits from R&D Systems, according to the manufacturer's instructions. Nitric oxide production was estimated in macrophage culture supernatants harvested at 24 h using the Griess method for nitrite quantification [50].

4.13. Acute Toxicity in Mice

Male BALB/c mice (6–8 weeks of age; $n = 6/\text{group}$) were randomized into three groups and treated orally with a single dose of **SintMed150** (50 or $100 \text{ mg}/\text{kg}$) or vehicle (solution containing 30% sorbitol, 10% Tween 80, and 60% saline). Animals were monitored for signs of general toxicity for 2 weeks after treatment. Observations involved changes in eyes, fur, and skin, and the occurrence of tremors, salivation, convulsions, diarrhea, sleep, lethargy, and coma. Body weights were taken and recorded at days 0, 7, and 14.

4.14. LPS-Induced Endotoxin Shock

Groups of five male BALB/c mice (4 weeks of age) were used for the LPS lethality assays. Mice were treated with different doses of **SintMed150** (50 or $100 \text{ mg}/\text{kg}$), dexamethasone ($25 \text{ mg}/\text{kg}$), or vehicle (solution containing 30% sorbitol, 10% Tween 80, and 60% saline), by intraperitoneal (i.p.) route. Ninety minutes later, animals were challenged with $600 \mu\text{g}$ of LPS (from serotype 0111:B4 *Escherichia coli*, Sigma-Aldrich) in saline, by i.p. route. The survival rate was then monitored daily during 4 days.

4.15. Induction of Acute Peritonitis in Mice

Male BALB/c mice (6–8 weeks of age; $n = 6/\text{group}$) were randomized into three groups and treated orally with **SintMed150** ($100 \text{ mg}/\text{kg}$), dexamethasone ($25 \text{ mg}/\text{kg}$), or vehicle (solution containing 30% sorbitol, 10% Tween 80, and 60% saline) 24 and 1 h before the challenge. Next, animals were challenged with a $250 \mu\text{L}$ injection of carrageenan ($1 \text{ mg}/\text{mL}$; intraperitoneal route). After 4 h, animals were euthanized and peritoneal exudates were harvested by peritoneal lavage using 2.5 mL of saline solution. Cells were centrifuged at $400 \times g$ for 10 min, at 4°C . The pellet was resuspended in saline (1 mL). Total leukocytes in the peritoneal fluid were determined in a Neubauer chamber after dilution in Trypan blue stain. Differential counting of neutrophils was carried out in rapid panotype-stained cytospin preparations. A differential count of 300 cells was made in a blinded fashion and according to standard morphologic criteria.

4.16. Statistical Analysis

To determine the cytotoxicity concentration of 50% of J774 macrophages (CC_{50}), we used non-linear regression. One-way analysis of variance and Newman-Keuls multiple comparison tests were employed by using Graph Pad Prism version 8.0.1 (Graph Pad Software; San Diego, CA, USA). Differences were considered significant when the values of p were < 0.05 . The data are representative of at least two or three experiments.

5. Conclusions

The investigation of the immunomodulatory potential of the series Fc-NAH has led to the successful discovery of 16 new bioactive molecules designed on the basis of molecular

hybridization, while some structure–activity relationships (SAR) have arisen from the analysis of the outcomes. A structural pattern seems to be closely associated with the most active compounds, namely the *ortho* substitution at the phenyl ring. Additionally, the presence of a phenyl ring appears to be essential for achieving better biological responses. The data presented here demonstrate that **SintMed** molecules can modulate the immune response in inflammatory conditions by decreasing the production of inflammatory mediators such as IFN- γ , IL-1 β , IL-2, nitric oxide, and TNF- α , without affecting cell viability. Furthermore, oral administration of the **SintMed150** derivative significantly increased the survival rate of mice in a model of endotoxic shock induced by LPS and decreased inflammatory cell migration in a peritonitis model induced by carrageenan. These findings suggest that the class of ferrocene-*N*-acyl hydrazones has therapeutic potential and may be useful in the development of drugs to treat inflammatory conditions.

Supplementary Materials: The following supporting information can be downloaded at: <https://www.mdpi.com/article/10.3390/molecules27238343/s1>, S2–S9: Characterization of the ferrocenyl-*N*-acyl hydrazones **SintMed(141–156)**, S10–S44: Spectroscopic data: NMR and IR spectra of Fc-NAH **SintMed(141–156)**, S45–S47: X-ray crystallographic data of **SintMed149**.

Author Contributions: L.P.S.: performed experiments, data analysis, and writing of the original draft of the manuscript. I.P.S.: performed experiments, instrument handling, acquisition, and analysis of data. D.K.C.S.: performed experiments and wrote the original draft of the manuscript. B.P.Z.C.d.R.: performed experiments, instrument handling, and data analysis. C.S.M.: conceived and designed the experiments and supervised them. M.V.B.d.S.C.: performed experiments and provided intellectual input into the study. J.M.d.S.F.: manuscript writing, editing, and formatting. J.H.d.A.-N.: performed experiments, acquisition, and analysis of data. J.A.E.: performed experiments, acquisition, and analysis. R.G.d.S.: analysis of data, manuscript writing and editing. M.B.P.S.: provided intellectual input into the study and proofread the manuscript. All authors have read and agreed to the published version of the manuscript.

Funding: This work was supported by grants from CNPq (grant numbers 562655/2010-7 and 312505/2021-3), FAPESP (grant numbers 2017/15840-0 and 2021/04876-4), and PRONEX (grant number 0002/2014).

Institutional Review Board Statement: Not applicable.

Informed Consent Statement: Not applicable.

Data Availability Statement: Not applicable.

Acknowledgments: The authors are grateful to Eliete de Fátima V. B. N. da Silva and the Analytical Centre of Fundamental Chemistry Department, Federal University of Pernambuco, for the NMR, IR, and elemental analysis experiments.

Conflicts of Interest: The authors declare no conflict of interest.

Abbreviations

CC₅₀: cytotoxicity concentration of 50%; COX: cyclooxygenase; IFN γ : interferon gamma; IL: interleukin; LPS: lipopolysaccharide; NAH: *N*-acyl hydrazones; NO: nitric oxide; NSAIDs: non-steroidal anti-inflammatory agents; TNF α : tumor necrosis factor alpha.

References

1. Chovatiya, R.; Medzhitov, R. Stress, inflammation, and defense of homeostasis. *Mol. Cell* **2014**, *54*, 281–288. [[CrossRef](#)] [[PubMed](#)]
2. Chen, L.; Deng, H.; Cui, H.; Fang, J.; Zuo, Z.; Deng, J.; Li, Y.; Wang, X.; Zhao, L. Inflammatory responses and inflammation-associated diseases in organs. *Oncotarget* **2017**, *14*, 7204–7218. [[CrossRef](#)] [[PubMed](#)]
3. Kuprash, D.V.; Nedospasov, S.A. Molecular and cellular mechanisms of inflammation. *Biochemistry* **2016**, *81*, 1237–1239. [[CrossRef](#)] [[PubMed](#)]
4. Seelaender, M.; Rosa-Neto, J.C.; Pimentel, G.D.; Goldszmid, R.S.; Lira, F.S. Inflammation in the disease: Mechanism and therapies 2014. *Mediat. Inflamm.* **2015**, *2015*, 169852. [[CrossRef](#)] [[PubMed](#)]

5. Alessandri, A.L.; Sousa, L.P.; Lucas, C.D.; Rossi, A.G.; Pinho, V.; Teixeira, M.M. Resolution of inflammation: Mechanisms and opportunity for drug development. *Pharm. Ther.* **2013**, *139*, 189–212. [[CrossRef](#)] [[PubMed](#)]
6. Ronchetti, S.; Migliorati, G.; Bruscoli, S.; Riccardi, C. Defining the role of glucocorticoids in inflammation. *Clin. Sci.* **2018**, *132*, 1529–1543. [[CrossRef](#)]
7. Bacchi, S.; Palumbo, P.; Sponta, A.; Coppolino, M.F. Clinical pharmacology of non-steroidal anti-inflammatory drugs: A review. *Antiinflamm. Antiallergy Agents Med. Chem.* **2012**, *11*, 52–64. [[CrossRef](#)]
8. Bindu, S.; Mazumder, S.; Bandyopadhyay, U. Non-steroidal anti-inflammatory drugs (NSAIDs) and organ damage: A current perspective. *Biochem. Pharmacol.* **2020**, *180*, 114147. [[CrossRef](#)]
9. Oray, M.; Samra, K.A.; Ebrahimiadib, N.; Messe, H.; Foster, C.S. Long-term side effects of glucocorticoids. *Expert Opin. Drug Saf.* **2016**, *15*, 457–465. [[CrossRef](#)]
10. Verma, G.; Marella, A.; Shaquiquzzaman, M.; Akhtar, M.; Ali, M.R.; Alam, M.M. A review exploring biological activities of hydrazones. *J. Pharm. Bioallied Sci.* **2014**, *6*, 69–80.
11. Guimarães, E.T.; Santos, T.B.; Silva, D.K.C.; Meira, C.S.; Moreira, D.R.M.; Silva, T.F.; Salmon, D.; Barreiro, E.J.; Soares, M.B.P. Potent immunosuppressive activity of a phosphodiesterase-4 inhibitor N-acylhydrazone in models of lipopolysaccharide-induced shock and delayed-type hypersensitivity reaction. *Int. Immunopharmacol.* **2018**, *65*, 108–118. [[CrossRef](#)] [[PubMed](#)]
12. Cequeira, J.V.; Meira, C.S.; Santos, E.S.; França, L.S.A.; Vasconcelos, J.F.; Nonaka, C.K.V.; Melo, T.L.; Filho, J.M.S.; Moreira, D.R.M.; Soares, M.B.P. Anti-inflammatory activity of SintMed65, an N-acylhydrazone derivative, in a mouse model of allergic airway inflammation. *Int. Immunopharmacol.* **2019**, *75*, 105735. [[CrossRef](#)]
13. Meira, C.S.; Filho, J.M.S.; Sousa, C.C.; Anjos, P.S.; Cerqueira, J.V.; Neto, H.A.D.; Silveira, R.G.; Russo, H.M.; Wolfender, J.L.; Queiroz, E.F.; et al. Structural design, synthesis and substituent effect of hydrazone-N-acylhydrazones reveal potent immunomodulatory agents. *Bioorg. Med. Chem.* **2018**, *26*, 1971–1985. [[CrossRef](#)] [[PubMed](#)]
14. Gundla, R.; Shaik, B.B.; Gorantla, V. *N-Acyl Hydrazones: Nonsteroidal Anti-Inflammatory Agents (NSAIDs)*, 1st ed.; LAP LAMBERT Academic Publishing: Hyderabad, India, 2021; pp. 1–112.
15. Kajal, A.; Bala, S.; Sharma, N.; Kamboj, S.; Saini, V. Therapeutic Potential of Hydrazones as Anti-Inflammatory Agents. *Int. J. Med. Chem.* **2014**, *2014*, 761030. [[CrossRef](#)] [[PubMed](#)]
16. De Melo, T.R.F.; Chelucci, R.C.; Pires, M.E.L.; Dutra, L.A.; Barbieri, K.P.; Bosquesi, P.L.; Trossini, G.H.G.; Chung, M.C.; Santos, J.L. Pharmacological Evaluation and Preparation of Nonsteroidal Anti-Inflammatory Drugs Containing an N-Acyl Hydrazone Subunit. *Int. J. Mol. Sci.* **2014**, *15*, 5821–5837. [[CrossRef](#)]
17. Medeiros, M.A.M.B.; Gama, E.; Silva, M.; De Menezes Barbosa, J.; Martins de Lavor, É.; Ribeiro, T.F.; Macedo, C.A.F.; De Souza Duarte-Filho, L.A.M.; Feitosa, T.A.; De Jesus Silva, J.; et al. Antinociceptive and anti-inflammatory effects of hydrazone derivatives and their possible mechanism of action in mice. *PLoS ONE* **2021**, *16*, e0258094. [[CrossRef](#)]
18. Viegas-Junior, C.; Danuello, A.; Bolzani, V.S.; Barreiro, E.J.; Fraga, C.A.M. Molecular hybridization: A useful tool in the design of new drug prototypes. *Curr. Med. Chem.* **2007**, *14*, 1829–1852. [[CrossRef](#)]
19. Ivasiv, V.; Albertini, C.; Gonçalves, A.E.; Rossi, M.; Bolognesi, M.L. Molecular Hybridization as a Tool for Designing Multitarget Drug Candidates for Complex Diseases. *Curr. Top. Med. Chem.* **2019**, *19*, 1694–1711. [[CrossRef](#)]
20. Singh, A.; Lumb, I.; Mehra, V.; Kumar, V. Ferrocene-appended pharmacophores: An exciting approach for modulating the biological potential of organic scaffolds. *Dalton Trans.* **2019**, *48*, 2840–2860. [[CrossRef](#)]
21. Altowyan, M.S.; Ali, M.; Soliman, S.M.; Al-Majid, A.M.; Islam, M.S.; Yousuf, S.; Choudhary, M.I.; Ghabbour, H.A.; Barakat, A. Synthesis, computational studies and biological activity of oxamohydrazone derivatives bearing isatin and ferrocene scaffolds. *J. Mol. Struct.* **2019**, *1202*, 127372. [[CrossRef](#)]
22. Guo, W.-Y.; Chen, L.-Z.; Shen, B.-N.; Liu, X.-H.; Tai, G.-P.; Li, Q.-S.; Gao, L.; Ruan, B.-F. Synthesis and in vitro and in vivo anti-inflammatory activity of novel 4-ferrocenylchroman-2-one derivatives. *J. Enzym. Inhib. Med. Chem.* **2019**, *34*, 1678–1689. [[CrossRef](#)] [[PubMed](#)]
23. Barišić, L.; Rošćić, M.; Kovačević, M.; Semenčić, M.Č.; Horvat, Š.; Rapić, V. The first ferrocene analogues of muramyl dipeptide. *Carbohydr. Res.* **2011**, *346*, 678–684. [[CrossRef](#)] [[PubMed](#)]
24. Soares, M.B.P.; Costa, J.F.O.; de Sá, M.S.; Ribeiro-dos-Santos, R.; Pigeon, P.; Jaouen, G.; Santana, A.E.G.; Goulart, M.O.F.; Hillard, E. Antiparasitic and immunomodulatory activities of 1,1-bis(4-hydroxyphenyl)-2-phenyl-but-1-ene and its protected and free 2-ferrocenyl derivatives. *Drug Dev. Res.* **2010**, *71*, 69–75. [[CrossRef](#)]
25. Chaudhary, A.; Poonia, K. The redox mechanism of ferrocene and its phytochemical and biochemical compounds in anticancer therapy: A mini review. *Inorg. Chem. Commun.* **2021**, *134*, 109044. [[CrossRef](#)]
26. Shoukat, H.; Altaf, A.A.; Badshah, A. Ferrocene-Based Metallodrugs. In *Advances in Metallodrugs: Preparation and Applications in Medicinal Chemistry*; Ul-Islam, S., Hashmi, A.A., Khan, S.A., Eds.; Wiley-Scrivener: Beverly, CA, USA, 2020; pp. 115–136.
27. Song, J.; Liu, H.; Lei, M.; Tan, H.; Chen, Z.; Antoshin, A.; Payne, G.F.; Qu, X.; Liu, C. Redox-Channeling Polydopamine-Ferrocene (PDA-Fc) Coating To Confer Context-Dependent and Photothermal Antimicrobial Activities. *ACS Appl. Mater. Interfaces* **2020**, *12*, 8915–8928. [[CrossRef](#)]
28. Larik, F.A.; Saeed, A.; Fattah, T.A.; Muqadar, U.; Channar, P.A. Recent advances in the synthesis, biological activities and various applications of ferrocene derivatives. *Appl. Organometal. Chem.* **2016**, *31*, e3664. [[CrossRef](#)]

29. dos Santos Filho, J.M.; Queiroz e Silva, D.M.A.; Macedo, T.S.; Teixeira, H.M.P.; Moreira, D.R.M.; Challal, S.; Wolfender, J.; Queiroz, E.F.; Soares, M.B.P. Conjugation of *N*-acylhydrazone and 1,2,4-oxadiazole leads to the identification of active antimalarial agents. *Bioorg. Med. Chem.* **2016**, *24*, 5693–5701. [[CrossRef](#)]
30. Mu, H.; Gong, R.; Ren, L.; Zhong, C.; Sun, Y.; Fu, E. An intramolecular charge transfer fluorescent probe: Synthesis and selective fluorescent sensing of Ag⁺. *Spectrochim. Acta Part A* **2008**, *70*, 923–928. [[CrossRef](#)]
31. dos Santos Filho, J.M. Mild, Stereoselective, and Highly Efficient Synthesis of *N*-Acylhydrazones Mediated by CeCl₃·7H₂O in a Broad Range of Solvents. *Eur. J. Org. Chem.* **2014**, *29*, 6411–6417. [[CrossRef](#)]
32. Lopes, A.B.; Miguez, E.; Kümmerle, A.E.; Rumjanek, V.M.; Fraga, C.A.M.; Barreiro, E.J. Characterization of Amide Bond Conformers for a Novel Heterocyclic Template of *N*-acylhydrazone Derivatives. *Molecules* **2013**, *18*, 11683–11704. [[CrossRef](#)]
33. da Silva, T.F.; Bispo Júnior, W.; Alexandre-Moreira, M.S.; Costa, F.N.; Monteiro, C.E.S.; Ferreira, F.F.; Barroso, R.C.R.; Noël, F.; Sudo, R.T.; Zapata-Sudo, G.; et al. Novel Orally Active Analgesic and Anti-Inflammatory Cyclohexyl-*N*-Acylhydrazone Derivatives. *Molecules* **2015**, *20*, 3067–3088. [[CrossRef](#)] [[PubMed](#)]
34. Thota, S.; Rodrigues, D.A.; Pinheiro, P.S.M.; Lima, L.M.; Fraga, C.A.M.; Barreiro, E.J. *N*-Acylhydrazones as drugs. *Bioorg. Med. Chem. Lett.* **2018**, *28*, 2797–2803. [[CrossRef](#)] [[PubMed](#)]
35. Cordeiro, N.M.; Freitas, R.H.C.N.; Fraga, C.A.M.; Fernandes, P.D. Discovery of Novel Orally Active Tetrahydro-Naphthyl-*N*-Acylhydrazones with In Vivo Anti-TNF- α Effect and Remarkable Anti-Inflammatory Properties. *PLoS ONE* **2016**, *11*, e0156271. [[CrossRef](#)] [[PubMed](#)]
36. Moraes, A.D.T.O.; Miranda, M.D.S.; Jacob, Í.T.T.; Amorim, C.A.D.C.; Moura, R.O.; Silva, S.Â.S.D.; Soares, M.B.P.; Almeida, S.M.V.; Souza, T.R.C.L.; Oliveira, J.F.; et al. Synthesis, in vitro and in vivo biological evaluation, COX-1/2 inhibition and molecular docking study of indole-*N*-acylhydrazone derivatives. *Bioorg. Med. Chem.* **2018**, *26*, 5388–5396. [[CrossRef](#)] [[PubMed](#)]
37. Chellan, P.; Sadler, P.J. Enhancing the Activity of Drugs by Conjugation to Organometallic Fragments. *Chem. Eur. J.* **2020**, *26*, 8676–8688. [[CrossRef](#)]
38. Dos Santos Filho, J.M.; Moreira, D.R.; De Simone, C.A.; Ferreira, R.S.; McKerrow, J.H.; Meira, C.S.; Guimarães, E.T.; Soares, M.B.P. Optimization of anti-*Trypanosoma cruzi* oxadiazoles leads to identification of compounds with efficacy in infected mice. *Bioorg. Med. Chem.* **2012**, *20*, 6423–6433. [[CrossRef](#)]
39. Guzik, T.J.; Korbout, R.; Adamek-Guzik, T. Nitric oxide and superoxide in inflammation and immune regulation. *J. Physiol. Pharm.* **2003**, *54*, 469–487.
40. Parameswaran, N.; Patial, S. Tumor necrosis factor- α signaling in macrophages. *Crit. Rev. Eukaryot. Gene Expr.* **2010**, *20*, 87–103. [[CrossRef](#)]
41. Lopez-Castejon, G.; Brough, D. Understanding the mechanism of IL-1 β secretion. *Cytokine Growth Factor Rev.* **2011**, *22*, 189–195. [[CrossRef](#)]
42. Rollas, S.; Küçükgülzel, S.G. Biological activities of hydrazone derivatives. *Molecules* **2007**, *12*, 1910–1939. [[CrossRef](#)]
43. Zeeshan, S.; Naveed, M.; Khan, A.; Atiq, A.; Arif, M.; Ahmed, M.N.; Kim, Y.S.; Khan, S. *N*-Pyrazoloyl and *N*-thiopheneacetyl hydrazone of isatin exhibited potent anti-inflammatory and anti-nociceptive properties through suppression of NF- κ B, MAPK and oxidative stress signaling in animal models of inflammation. *Inflamm. Res.* **2019**, *68*, 613–632. [[CrossRef](#)] [[PubMed](#)]
44. Debnath, U.; Mukherjee, S.; Joardar, N.; Sinha Babu, S.P.; Jana, K.; Misra, A.K. Aryl quinolinyl hydrazone derivatives as anti-inflammatory agents that inhibit TLR4 activation in the macrophages. *Eur. J. Pharm. Sci.* **2019**, *134*, 102–115. [[CrossRef](#)]
45. Kohno, K.; Kataoka, J.; Ohtsuki, T.; Suemoto, Y.; Okamoto, I.; Usui, M.; Ikeda, M.; Kurimoto, M. IFN- γ -inducing factor (IGIF) is a costimulatory factor on the activation of Th1 but not Th2 cells and exerts its effect independently of IL-12. *J. Immunol.* **1997**, *15*, 1541–1550.
46. Boyman, O.; Sprent, J. The role of interleukin-2 during homeostasis and activation of the immune system. *Nat. Rev. Immunol.* **2012**, *17*, 180–190. [[CrossRef](#)] [[PubMed](#)]
47. Sheldrick, G.M. SHELXT—Integrated space-group and crystalstructure determination. *Acta Crystallogr. Sect. A Found. Adv.* **2015**, *71*, 3–8. [[CrossRef](#)] [[PubMed](#)]
48. Sheldrick, G.M. Crystal structure refinement with SHELXL. *Acta Crystallogr. Sect. C Struct. Chem.* **2015**, *71*, 3–8. [[CrossRef](#)] [[PubMed](#)]
49. Puschmann, H.; Bourhis, L.J.; Dolomanov, O.V.; Gildea, R.J.; Howard, J.A.K. OLEX2—A complete package for molecular crystallography. *Acta Crystallogr. Sect. A Found. Crystallogr.* **2011**, *67*, C593. [[CrossRef](#)]
50. Green, L.C.; Wagner, D.A.; Glogowski, J.; Skipper, P.L.; Wishnok, J.S.; Tannenbaum, S.R. Analysis of nitrate, nitrite, and [¹⁵N]nitrate in biological fluids. *Anal. Biochem.* **1982**, *126*, 131–138. [[CrossRef](#)]